Changes in the vegetation and water cycle of the Ecuadorian páramo during the last 5000 years

Marie-Pierre Ledru, Olga Aquino-Alfonso, Walter Finsinger, Pablo Samaniego, Silvana Hidalgo

The Holocene

Changes in the vegetation and water cycle of the Ecuadorian páramo during the last 5000 years

Journal:	*The Holocene*
Manuscript ID	HOL-22-0006.R1
Manuscript Type:	Paper
Date Submitted by the Author:	12-Apr-2022
Complete List of Authors:	Ledru, Marie-Pierre; Institut de Recherche pour le Développement France-Sud, ISEM (Univ Montpellier CNRS EPHE IRD) Aquino Alfonso, Olga; Université de Montpellier, ISEM Finsinger, Walter; CNRS, ISEM; Samaniego, Pablo; Institut de Recherche pour le Développement France-Sud, Laboratoire Magmas et Volcans, Univ Clermont Auvergne, CNRS, IRD Hidalgo, Silvana; Escuela Politecnica Nacional Instituto Geofisico
Keywords:	Tropical Andes, fire, tephra, SASM, adiabatic upslope, soil moisture
Abstract:	We analyzed changes in the long-term vegetation cover and in fire activity over the past 5,000 years in the Ecuadorian páramo using a sediment core from Papallacta (Ecuador). The chronology is constrained by three tephra layers and 32 AMS 14C ages, and 168 samples yielded a high-resolution record of environmental changes. We estimated the upslope wind convectivity as the ratio between pollen transported from the Andean cloud forest and Poaceae pollen to distinguish changes in atmospheric moisture from changes in soil moisture. The record showed that the two sources of moisture, either from year-round adiabatic cloud dripping linked to SASM activity or to ENSO variability at decadal-scale, influenced vegetation-cover changes. Between 5000 and 2450 cal yr BP, both soil moisture and biomass burning were higher than after 2450 cal yr BP. The shift between the two states matches the zonal increase in summer insolation that drove the ITCZ to its southernmost position. Our results underline resilience to volcanic activity, the importance of the upslope convective dripping with the lowest convective index observed at ~4500 cal yr BP, the anomalous last century with the highest convective activity and the driest soil conditions recorded in the last 5000 years, the recent increase in fire activity and the link between soil moisture and the position of the ITCZ.

Changes in the vegetation and water cycle of the Ecuadorian páramo during the last 5000 years

Marie-Pierre Ledru[1], Olga Aquino-Alfonso[1], Walter Finsinger[1], Pablo Samaniego[2], Silvana Hidalgo[3]

1, ISEM Univ Montpellier CNRS IRD EPHE, Montpellier, France
2 Laboratoire Magmas et Volcans, Univ Clermont Auvergne, CNRS, IRD, Aubière, France
3 Instituto Geofísico, Escuela Politécnica Nacional, Quito, Ecuador

Keywords: Tropical Andes, fire, tephra, SASM, adiabatic upslope, soil moisture

Abstract

We analyzed changes in the long-term vegetation cover and in fire activity over the past 5,000 years in the Ecuadorian páramo using a sediment core from Papallacta (Ecuador). The chronology is constrained by three tephra layers and 32 AMS ^{14}C ages, and 168 samples yielded a high-resolution record of environmental changes. We estimated the upslope wind convectivity as the ratio between pollen transported from the Andean cloud forest and Poaceae pollen to distinguish changes in atmospheric moisture from changes in soil moisture. The record showed that the two sources of moisture, either from year-round adiabatic cloud dripping linked to SASM activity or to ENSO variability at decadal-scale, influenced vegetation-cover changes. Between 5000 and 2450 cal yr BP, both soil moisture and biomass burning were higher than after 2450 cal yr BP. The shift between the two states matches the zonal increase in summer insolation that drove the ITCZ to its southernmost position. Our results underline resilience to volcanic activity, the importance of the upslope convective dripping with the lowest convective index observed at ~4500 cal yr BP, the anomalous last century with the highest convective activity and the driest soil conditions recorded in the last 5000 years, the recent increase in fire activity and the link between soil moisture and the position of the ITCZ.

Introduction

Páramo (or páramos) is a widespread treeless grassland neotropical ecosystem located in the wetter northern Andes (Borrelli et al., 2015) between the upper limit of the cloud forest (*c.* 3,000 m asl) and the upper limit of plant life (*c.* 4,700 m asl; Luteyn 1999; Körner and Paulsen, 2004). Páramos play an important ecological role in regional water storage (Buytaert et al., 2006) and in the global carbon balance and host high biodiversity (Zúñiga-Escobar et al., 2013). Water drains from the wetlands into the thick volcanic soils that form the "sponge" of the páramo, where the precipitation is stored. Currently, tussock grassland (*Calamagrostis* sp or/and *Festuca* sp), acaulescent rosettes and cushions, the dominant growth forms of the páramo (Ramsay and Oxley, 1997), are undergoing severe degradation due to burning and grazing (Grub et al., 2020). Degraded areas only recover slowly due to the high elevation as well as the effects of the oxygen level, high radiation and drying wind; as a result, the high biodiversity of this ecosystem is under threat. An additional issue is ongoing and future climate change with increasing temperatures and the associated glacier retreat and an increase in drought events and in fire frequency due to enhanced precipitation seasonality (Urrutia and Vuille, 2009).

The long-term management of the páramo requires a detailed understanding of the role of fire (Sarmiento and Frohlich, 2002). While the grasslands are highly flammable, their ability to sprout and germinate after fires can be viewed as is considered as an adaptation to disturbance by fire (Borrelli et al., 2015; Horn and Kapelle, 2009). Accordingly, direct observations of lightning strikes and palaeoecological evidence of fires both clearly demonstrate that fires occur in neotropical páramo without human intervention (Horn and Kapelle 2009). However, the extent to which the páramo can be viewed as a fire-dependent ecosystem is still a matter of debate (Horn and Kappelle, 2009). Today, fire frequency in the páramo is higher than before, probably due to human-set fires that are used to remove the dead standing biomass of native grasses and promote the growth of young grass shoots that are easier to stock (Matson and Bart 2013).

Long-term palaeoecological records from natural archives (lacustrine sediments, peat) make it possible to document vegetation responses to climate and fire-regime changes under environmental conditions that differ substantially from those that occurred during the historical period. For instance, in Colombia, the upper tree line shifted in conjunction with glacier advances and retreats during the glacial-interglacial cycles over the Quaternary (Hooghiemstra and Flantua, 2019). During the Holocene, at millennial time scales, the South American Summer Monsoon (SASM) gradually intensified in response to increasing southern hemisphere summer insolation. Thus, during the mid-Holocene (7000 to 5000 yr BP), a weaker SASM system produced drier conditions in large parts of the neotropics south of the equator (Prado et al., 2013; Valencia et al., 2018). Further north, near the Pacific coast of Ecuador, the strengthening of the cold Humboldt current led to cooler climatic conditions between 4200 and 2850 cal BP (Seillès et al., 2015) and drier conditions in the Ecuadorian Andes between 5500 and 2500 cal yr BP (Rodbell et al., 1999) when the InterTropical Convergence Zone (ITCZ) was in its northernmost position. Andean pollen records for the late Holocene rather centered on changes in the upper forest

limit, with the highest position reached around 4900 cal yr BP in conjunction with wetter climate conditions and the lowermost altitude reached between ~910 and 520 cal yr BP in conjunction with drier climate conditions (Bakker et al., 2008; Jansen et al., 2013). Similarly, little is known about the floristic changes of the páramo.

Here we present new high-resolution pollen and macroscopic charcoal records spanning the past 5,000 years from a peat bog (Papallacta) located in the páramo of Antisana, one of the main hydrological basins for Quito, the capital city of Ecuador (Buytaert et al., 2006). The pollen record from this site for the last 1,000 years showed that vegetation was highly sensitive to moisture from two main sources, one the annual amount of rainfall retained in the soil, and the other from the upslope cloud convection that delivers moisture from the Amazon basin to the summits (Ledru et al., 2013). By extending the Papallacta record further back in time, we explore the longer-term drivers of changes in hydrological conditions, fire and vegetation in a high elevation ecosystem in the tropics.

Study area

The Papallacta (or Sucus) peat bog is located on the eastern part of the Chacana volcanic complex, and at 12-14 km to the north slope of the Antisana volcano at an elevation of 3,815 m asl (00º2'30" S, 78º11'37" W) on the Eastern Cordillera range (EC) (Fig. 1A). The Antisana (5,704 m asl) is a potentially active volcano in the Ecuadorian Eastern Cordillera, whose most recent fumarolic activity was reported by Humboldt at the beginning of the 19th century (Hall et al., 2017). Antisana's base diameter is ca. 14 km, running north-south. There, glaciers descend to approximately 4,600 m (eastern side) and 4,800 m (western side), while older moraines dated to the Younger Dryas cold event indicate glaciers about 1,200 m lower on the eastern side (Hastenrath, 1981; Clapperton et al., 1997). Average annual temperature is between 7.5 ºC (at 3,500 m asl) and 5 ºC (at 4,000 m asl) (Jorgensen and Leon-Yanez, 1999).

The climate in the equatorial Andes is influenced by complex and heterogeneous atmospheric mechanisms (Segura et al., 2019). Currently, both the Eastern (EC) and the Western Cordillera (WC) are under the seasonal influence of the Intertropical Convergence Zone (ITCZ), a zone of deep convection that produces heavy precipitation due to the convergence of the trade winds at low latitudes between February and April (Garreaud, 2009). The EC receives year-round rainfall fed by moist air resulting from evapotranspiration of the trees in the Amazon basin (Bendix et al., 2006a, 2006b). Upon meeting the Andes, these moist air masses ascend, cool, and lose a substantial portion of their humidity (orographic rain) thereby attenuating the dry season. As a result, large parts of the EC are currently characterized by the absence of a dry season (Fig. 1B). However, extreme monthly wet (dry) events are associated with anomalous southward (northward) shifts of the eastern pacific ITCZ during the rainy season (Segura et al., 2019).

Today, at the high elevation of the Papallacata bog on the north-western slope of the Antisana, two main mechanisms are responsible for the year-round precipitation: regular SASM activity observed every

year and variable El Niño activity (Vuille and Werner 2005). First, the South American Summer Monsoon (SASM) is paced by the southward migration of the ITCZ over the tropical Atlantic and Pacific Oceans during austral summer and causes precipitation during the austral summer (Fig. 1A; Ledru et al., 2013). Second, the interannual variability in precipitation related to ENSO (El Niño Southern Oscillation) with El Niño (La Niña) episodes associated with warmer (cooler) and below (above) average rainfall in the Amazon Basin (Marengo and Nobre, 2001; Marengo, 2009) as well as glacier regression (expansion) in Ecuador (Caceres et al., 2006). At millennial scale, paleoclimatic records reconstructed mean-state variations in ENSO-like behavior, for instance, in the lacustrine sediment of the Galapagos with an increase in ENSO variability in the Late Holocene (Moy et al., 2002; Conroy et al., 2009; Zhang et al., 2014).

Sucus bog, located close to the town of Papallacta, hereafter named Papallacta bog, is a wetland area located within the páramo. Patches of *Polylepis* forest grow on the slopes above the bog (Fig. 1C). In the region of Antisana, the cloud forest (or upper montane rain forest) occurs between *ca.* 2,500 m a.s.l. and 3,400-3,600 m a.s.l. and is mainly dominated by *Weinmannia pinata, Schefflera sodiroi, Myrcianthes rhopaloides, Hedyosmum cumbalense, H. luteynii, Oreopanax ecuadoriensis, Hesperomeles ferruginea,* and *Weinmannia fagaroides.* Between 3,600 and 4,300 m asl, in the Páramo, *Gynoxys acostae, Escallonia myrtilloides, Buddleia, Polylepis* are observed and, high elevation, or super páramo extends between 4,200 and 4,600 m on the eastern side. Shrubby vegetation dominated by *Loricaria antisanensis* grows on the eastern humid side at *ca.* 4,200 m (Sklenar and Jorgensen, 1999) (Table 1).

Table 1. Description of the vegetation cover around Papallacta bog (from Ledru et al., 2013).

Site	Family	Species	Family	Species
Paramo 3,600- 4,000 m asl	Poaceae	*Calamagrostis*	Asteraceae	*Diplostephium*
		Festuca		
	Rosaceae	*Polylepis*		*Pentacalia*
	Hypericaceae	*Hypericum*		
Papallacta bog 3,815 m asl	Asteraceae	*Loricaria toyoides*	Gunneraceae	*Gunnera magellanica*
		Dorobaea pinpinelifolia	Ranunculaceae	*Ranunculus sp.*
		Monticalia vaccinioides	Clusiaceae	*Hypericum laricifolium*
		Hippochoeris sp.		*Hypericum sp.*
		Xenophyllum sp.	Geraniaceae	*Geranium sp.*
		Werneria sp.	Polygonaceae	*Muehlenbeckia volcanica*
	Valerianaceae	*Valeriana microphylla*	Apiaceae	*Hydrocotyle*
	Lycopodiaceae	*Huperzia sp.*		*Azorella*
	Gentianaceae	*Gentiana sedifolia*	Plantaginaceae	*Plantago rigida*
		Halemia weddeliana	Cyperaceae	*Carex lechmanii*
		Gentianella sp.		
	Poaceae	*Cortaderia sericanta*		

		Bromus sp.		
		Cortaderia nitida		
Cushion paramo	Apiaceae	*Azorella*	Plantaginaceae	*Plantago*
Paramo >4,000 m asl	Malvaceae	*Nototriche*	Brassicaceae	*Draba*
	Apiaceae	*Azorella*	Plantaginaceae	*Plantago*
	Asteraceae	*Chuquiraga*		
		Loricaria		
		Werneria		

Material and methods

Coring

The 9-m long sediment core named PA1-08 was collected from Papallacta peat bog in 2008 using a Russian-type corer (drives 1 m long, diameter 5 cm) (Fig. 1D). Sediment drives were transferred onto PVC half-tubes and sealed in a plastic sheath (Fig. 2). The sediments were then sliced into 2-cm thick slices, which were placed individually in labelled plastic bags and stored at +4 ºC at the University of Montpellier.

Chronology

A total of 34 bulk sediment samples were sent for radiocarbon Accelerator Mass Spectrometry (AMS) dating and measured at the *Laboratoire de Mesure du Carbone14* (LMC14)–UMS 2572 (CEA/DSM – CNRS–IRD–IRSN–*Ministère de la Culture et de la Communication*, Saclay, France), and at the BetaAnalytics laboratory (USA). In addition to radiocarbon dating, we used tephrochronology when tephra layers resulting from known volcanic eruptions were available. Tephrochronology is used to determine the age of a volcanic eruption based either on evidence from a historical archive or from prior dating of tephras in other sediment records (Turney and Lowe, 2001). The geochemical and mineralogical composition of the main of the tephra layers makes it possible to identify the origin of the uppermost ash layers (Table 3). However, our knowledge of the origin of the eruption and its corresponding ages become uncertain as one goes deeper in time (Table S1). We classified the tephra layers recognized in PA1-08 in three categories, from 0 for no uncertainty to 3 for maximum uncertainty, and only the three most recent tephra layers were usable for our age model (Table S2).

The chronology of the core was determined using rBacon v2.5.6 (Blaauw et al., 2021). It is constrained by 35 control points: 31 ^{14}C dates, the estimated age of the sediment surface (Table 2), and the ages of the three most recent tephra layers identified (Fig. 2). Three ^{14}C dates that were taken near sediment-drive ends were rejected as they reported much younger ages than expected based on adjacent dates. We excised sediments identified as tephra layers before age-modeling (and added them after age-modeling) as these sections are assumed to be abrupt accumulations. All ^{14}C dates were calibrated with a mixed

calibration curve (50% IntCal20 and 50% SHCal20) as the study site receives a mixture of northern and southern air masses (Hogg et al., 2020).

Charcoal analysis

We took a total of 322 samples, 69 of which originated from tephra layers, from the contiguous 2-cm thick sediment slices down to a depth of 700 cm, measured sample volumes by water displacement (median volume = 1 cm^3; range: 0.1-4 cm^3), and then soaked the samples in a 7.5% hydrogen peroxide solution for at least 24 hours (Schlachter and Horn, 2010) before gently washing them through a sieve with a 125 μm screen. To quantify charcoal abundances, we transferred the sieving residues into a white porcelain evaporating dish to facilitate the identification and counting of charcoal particles against the white background (Finsinger et al., 2014) and identified charcoal particles under a Leica M80 stereomicroscope at 7.5-60x magnifications based on the following features: dark, shiny and geometric particles that are brittle at low less pressure (Whitlock and Larsen, 2001). As charcoal morphology helps interpret the fuel source (Jensen et al., 2007; Feurdean, 2021), we counted charcoal pieces of Poaceae tissues (Jensen et al., 2007; Courtney-Mustaphi and Pisaric, 2014), wood and bark (types C and S in Enache and Cumming, 2006), and other charcoal morphologies ('undiff. charcoal') in 178 samples (34 of which were included in tephra layers). In addition, we scanned the samples at 7.5x magnification with a CMEX-5000 camera using the winSEEDLE™ software v2009 (Regent Instruments Canada Inc.) to measure both the total charcoal abundance and the cumulative sum of charcoal-particle areas (i.e., total charcoal per area) (Finsinger et al., 2014). To account for varying sediment accumulation rates, we selected the samples that were not included in tephra layers and calculated the charcoal accumulation rates (CHAR, pieces cm^{-2} yr^{-1}) based on the chronology (Whitlock and Larsen, 2001).

To determine the centennial-scale trends in CHAR, which was interpreted as reflecting the amount of biomass burned over time (Marlon et al. 2008; Higuera et al. 2010), and to identify peaks, which were interpreted as fire episodes, we analyzed the CHAR data using CharAnalysis v1.1 (Higuera et al., 2009). The analysis involved binning the charcoal record to a constant sampling resolution (here, the 3rd quartile value of the records' sampling resolution = 23 years $sample^{-1}$), decomposing that record into a background trend and a peak component using a lowess smoother robust to outliers (with a 500-year smoothing window), and evaluating peak samples using the 99th percentile of the modeled noise distribution obtained with a Gaussian mixture model and a peak-screening test (Higuera et al., 2009). The suitability of the record for peak detection was assessed with the signal-to-noise index (SNI; Kelly et al. 2011). We calculated fire return intervals (FRI) using the screened peak record.

Pollen analysis

A total of 200 pollen samples were taken from the 2-cm thick sediment slices down to a depth of 700 cm, 37 of which were taken from tephra layers. We measured both their wet and dry weights before processing the samples using a standard protocol (Faegri and Iversen, 1989). We mounted the residue in silicone oil on microscope slides and identified and counted a minimum of 300 terrestrial pollen grains in each sample under 630x magnification. Pollen grains and spores were identified using the ISEM reference pollen collection and pollen keys (Hooghiemstra, 1984; Ortuño, 2008; Kuentz, 2009; Herrera, 2010). Pollen taxa assignments to ecological groups (bog, Andean forest, páramo) were based on published classifications of páramo pollen records (Moscol Olivera et al., 2009; Moscol Olivera and Hooghiemstra, 2010) and on our own botanical survey (Ledru et al., 2013). To calculate percentages fern spores and aquatic or water level-related taxa were excluded from the total sum. The concentration of pollen was calculated using the method of Cour (1974). Pollen assemblage zones were determined by optimal partitioning with square-root transformed percentage values for pollen types included in the pollen sum (Birks and Gordon, 1985) and for all pollen samples, including those taken from tephra layers. Statistically significant zones were assessed by comparison with the broken-stick model, following Bennett (1996). Pollen diagrams and zonation were prepared with Psimpoll v4.26 (Bennett 2008).

To qualitatively estimate variations in convective wind activity over time we used the log-transformed Transported pollen: Poaceae pollen ratio (Ledru et al., 2013). According to our modern pollen survey, the pollen produced by three tree taxa that occur in the upper montane cloud forest (*Alnus, Hedyosmum, Podocarpus)* is transported upslope and characterizes the convective wind activity (Bendix et al., 2006c). Poaceae pollen frequency is related to the soil moisture of the páramo as plants of this family (*Calamagrostis, Festuca*) grow mainly on humid organic clayey soils (Liu et al 2005).

Table 2. Radiocarbon dates of core PA1-08. Radiocarbon ages were measured on total organic matter. * = calendar age; ** = rejected 14C dates

Lab number	Depth cm	Age ^{14}C yr BP	Lab number	Depth cm	Age ^{14}C yr BP
surface	0-2	-60 ±10*			
SacA-11045	22-24	0 ±30	SacA-11050	494-496	3305±30
SacA-18852	50-52	175±30	SacA-18857	516-518	3180±40
Beta-243042	80-82	270±40	SacA-14728	524-526	3790±35
SacA-14722	114-116	530±30	SacA-11051	548-550	3690±30
SacA-14723	160-162	1005±30	SacA-18858	554-556	3790±30
SacA-11046	186-188	1000±30	SacA-14677	568-570	3950±40
SacA-11047	208-210	1105±30	SacA-11052	594-596	3570±30**
SacA-14724	254-256	1540±35	Beta-243043	602-604	3440±40**
SacA-18853	284-286	1860±30	SacA-14678	636-638	4475 ±40
SacA-18855	322-324	2225±40	SacA-18859	680-682	4330±30

SacA-11048	338-340	2470±30	SacA-14679	712-714	4600 ±50
SacA-18854	350-352	2440±30	SacA-18860	742-744	4560±40
SacA-14725	386-388	2885±35	SacA-11053	766-768	4380±30
SacA-14726	404-406	2520±35	SacA-18861	788-790	4460±35
SacA-11049	438-440	2950±30	SacA-14729	806-808	4430±40
SacA-18856	450-452	2885±30	SacA-14680	832-834	4290±40
SacA-14727	476-478	2935±35	SacA-11054	862-863	3620±30**

Table 3 Description of the tephra layers observed in PA1-08 and reported in figure 3 together with the origin and the year of the eruption re-calculated from our age model (see also supplementary Tables 1 and 2). WC Western Cordillera, EC Eastern Cordillera.

Tephra layer number	Depth cm	Cordillera	Volcano	Calibrated date of the eruption	Description of the ash layer	References
M1	110-115	WC	Guagua Pichincha	1600 AD	Fine, yellowish ash	Robin et al., 2008
M2a & b	130-148	WC	Quilotoa	1150 AD	2a white & 2b coarse grey ash with small pumice lapilli	Mothes and Hall 2008
M3	181	WC	Guagua Pichincha	975 AD	Coarse, crystal-rich ash with peat	Robin et al., 2008
M4	202-206	EC	Cotopaxi?	1165 yr BP	Yelllowish ash	Hall and Mothes 2008
M5	208-226	EC	Antisana	1180 yr BP	Peat with coarse ash and disseminated lapilli	
M6	232-236	-	-	1235 yr BP	Fine, yellowish ash with peat	
M7	257-264	EC	Cotopaxi?	1460 yr BP	Coarse, crystal-rich ash with peat	
M8	318-322	-	-	2230 yr BP	Fine-medium, grey-yellow, crystal-rich ash with peat	
M9	326-332	WC	Atac	2290 yr BP	Fine, white ash	Hidalgo et al., 2008
M10	350-354	-	-	2445 yr BP	Medium ash with peat	
M11a	374-377	-	-	2560 yr BP	Fine, grey-yellowish ash	
M11b	381-386	WC	-	2585 yr BP	Fine, grey-yellowish ash with disseminated lapilli	
M12	458-464	-	-	3140 yr BP	Fine-medium, white ash, well-stratified oxidation level	Hildebrandt 1989
M13	470-473	EC	Tungurahua	3195 yr BP	Medium ash with peat	Hall et al., 1999; Le Pennec et al., 2013
M14	493-500	-	-	3500 yr BP	Fine, clay-rich, dar ash with peat	
M15	521-528	WC	Pichincha	3890 yr BP	Medium, grey-white ash with disseminated crystals	Robin et al., 2008
M16	538-542 546-562	EC	Cotopaxi	4075 y BP	Fine-medium, pseudo-stratified ash with disseminated lapilli	Hall and Mothes 2008
M17a	589-592	WC	-	4320 yr BP	Fine, white ash	
M17b	594-596	WC	-	4335 yr BP	Medium, grey-yellowish ash	
M18	658-668	EC	Atacazo-Ninahuilca	4790 yr BP	Fine, white ash	Hidalgo et al., 2008

Results

Lithology and chronology

The core was mostly composed of brown peat intercalated with 18 tephra layers, M1 to M18, corresponding to fine-to-medium sized distal ash deposits reported in Fig 2 and Table 3. The six radiocarbon dates below a depth of 700 cm are incoherent for regular sedimentation because they report similar ages (Table 2, Fig. 2). For this reason and based on evidence of a two-meter-thick homogeneous sediment layer composed of reworked organic mud and tephra, we interpreted these 2 m-layers of

sediment as a fluvio-glacial deposit. While this interpretation is weakly constrained, the chronology of the sediments above a depth of 700 cm is better constrained. The depth-age model shows that sediments accumulated at least over the past 5,000 years with relatively high sediment deposition times (1.5-20 yr cm^{-1}). Comparison of the age distributions of the tephras resulting from the depth-age model and published radiocarbon dates from within the tephra and/or paleosoils located below or above the tephras in the area of the volcanoes shows good coherence except when two different eruptions occurred within a short time interval (Table 3, Table S1).

Vegetation dynamics and fire history

The results of the pollen record are presented in a synthetic diagram along a depth scale (Fig. 3) and an age scale (Fig. 4). A total of 189 taxa were identified, including 56 tree pollen taxa, 84 non-arboreal pollen taxa, 27 fern taxa, 2 Algae and 22 unknown types. The Papallacta pollen diagram contains eight statistically significant pollen assemblage zones (Fig. 3 and 4). The signal-to-noise index (SNI) values (median SNI = 10.07, minimum SNI > 3) show that the charcoal-accumulation rate (CHAR) record is suitable for peak analysis and for the detection of fire events.

Pollen zone P1, (700-630 cm, 4960-4600 cal yr BP, 25 samples, resolution 14 years / sample)

This zone contained one 10-cm thick tephra deposit M18 (668-658 cm) dated to 4790 cal yr BP. The vegetation was dominated by Poaceae (35-72 %) with low pollen frequencies of cloud forest taxa *Alnus* (0.5 – 4.5%), *Hedyosmum* (1-8%), *Podocarpus* (0-1%). Among the non-arboreal taxa, *Ambrosia* (0-5%), *Gentianella* (0.2 – 1.5%) Ericaceae (0.2-5%) *Gunnera* (0.2 – 4%), *Acalypha* (0.3 – 5%), Cyperaceae (7-166%) with the highest frequencies at the top of the zone between 658 and 630 cm and the fern *Huperzia* (10- 95%). The quantity of burned biomass increased and two fire events were detected (Fig. 5). Charcoal morphotypes indicate that fires were fed by a mixture of wood and Poaceae fuel.

The beginning of the record, between 700 and 658 cm, was characterized by the presence of *Ambrosia*, bog plant assemblages and a few Cyperaceae, an assemblage that documents sufficent soil moisture. After the M18 tephra were deposited, Poaceae pollen frequency decreased while that of Cyperaceae increased.

Pollen Zone P2, 630-614 cm, 4600 – 4475 cal yr BP, 5 samples, resolution 25 years / sample

No tephra was deposited in this zone. Pollen assemblages were characterized by low frequency of Poaceae (6%), and high frequency of Ast *Senecio* (67%). *Melastomataceae* and *Polylepis* peaked towards the beginning of the zone (14% and 8%, respectively), while Apiaceae pollen values peaked towards the end of zone (20%). The upper montane cloud forest taxa (*Alnus, Hedyosmum, Podocarpus*) were well represented. The decrease in bog moisture-related taxa that started at the end of P1 (*Piper, Gunnera, Gentianella, Cyathea* and *Huperzia*) suggest drier conditions in the bog. Cyperaceae almost disappeared (~8%). Less biomass was burned and the fire-return interval (FRI) was slightly higher than in the previous zone.

Pollen Zone P3, 614-353 cm, 4475 – 2440 cal yr BP, 49 samples, resolution 41 years /sample

Seven tephra layers (M17 to M11) were deposited on the bog during this zone (Fig. 2, Table 3). Poaceae pollen was frequent but a sharp decrease was observed at 490 cm (3450 cal yr BP) (53% to 14%), and remained low up to 416 cm (2800 cal yr BP). This event lasted ~650 years then increased progressively to 68% (2575 cal yr BP) at the end of the zone, reaching 53% at 2440 cal yr BP. Poaceae (25-85%), Ast liguliflorae (0-6%) (Apiaceae 0-8%) *Alnus* (0-5%) *Hedyosmum* (0-4.5%) were the main taxa in pollen zone P3. While burned biomass was mostly low in this zone, distinct charcoal peaks point to the occurrence of fire events. The lowest FRI values (50 years) occurred around 3100-3050 cal yr BP when Poaceae pollen decreased. Charcoal morphotypes indicate that fire events around 4400-3800 and at 2600 cal BP were predominantly fuelled by Poaceae. The fire events at 4100 and 2550 cal yr BP occurred after tephra deposition (the ~40 cm thick M16 tephra and the 8 cm thick M11 tephra, respectively).

Pollen zone P4, 353- 280 cm, 2440-1685 cal yr BP, 24 samples, 31 years / sample

Two 4-cm thick tephra layers (M9 and M8) were deposited in a short time interval between 2290 and 2230 cal yr BP. The zone was characterized by a sharp decrease in Poaceae (16-42%) and in cloud forest-related tree taxa although the decrease in *Alnus* (0-3%) is masked by an increase in *Hedyosmum* (3-11%), an increase in Ast. *Senecio* (6-25%) including a decrease during the eruptions and at the end of the zone (0-3%). Cyperaceae disappeared progressively while *Thalictrum* (%), an herb of the paramo, increased. *Ambrosia* began to increase at the end of the zone (0-1% to 4-12%) while *Huperzia* increased right after the volcanic eruptions. The quantity of burned biomass remained low throughout the period and no fire event occurred. During this 750 yr interval, the convective activity index increased (Fig. 5) and *Polylepis* was well represented. This suggests no changes in the cloud and *Polylepis* forests but rather in the local assemblages with drier soil conditions after the two ash fallout deposits, as indicated by the increase in Apiaceae, which ranged from 0-1% before ash deposits and from 6-21% after the ash deposits, by the decrease in Ast. *Senecio* (25-3%), *Gunnera* frequency which was notable (6-3%) before the eruption and absent after the eruption (0-1%), by the increase in *Gentianella* (1-18%) which started just before the volcanic eruption, and by a brief increase in Poaceae during the interval of the volcanic eruption.

Pollen Zone P5, 280-200 cm, 1685 - 1155 cal yr BP, 22 samples, resolution 24 years / sample

Zone 5 lasted 530 years and included four tephra layers M7 (264-257 cm) and M6 (236-232 cm), M5 (226-208 cm) and M4 (206-202 cm) dated to 1460, 1235, 1180 and 1165 cal yr BP, respectively. No major changes in the ecology of the páramo occurred during and after the ash fallout deposits.

Pollen content was characterized by *Ambrosia* (5-20%), a decrease in Apiaceae (17-1%), a progressive decrease in *Huperzia* (62-4%), two peaks of *Gunnera* 33-36% at 248-246 cm (~1350 cal yr BP) and 11-20% at 208-210 cm (1180 cal yr BP), the second located above the M4 tephra deposition.

The sharp decrease in convective activity that started at the beginning of P5 was accentuated by the decrease in *Hedyosmum* (7-1%) observed at 250 cm (1375 cal yr BP). While burned biomass remained low, FRI dropped sharply to around 150-200 years.

Pollen Zone P6, 200-141 cm, 1155 – 770 cal yr BP, 21 samples, resolution 18 years / sample

Two tephra layers were deposited, M3 (181 cm) dated to 975 AD and the beginning of M2 (148-130 cm) dated to? 1150 AD. The pollen assemblages were characterized by *Ambrosia* (6-18%) and Poaceae (12-42%) both well represented throughout the zone, a decrease in Apiaceae (4-0%) and *Gentianella* (5-1%), a peak in Urticales (32 and 18%) before and after M3. Charcoal particles remained low with a decrease in the middle of the P6 zone. The convective activity index first increased in zone 6 before stabilizing. No changes occurred in the pollen assemblages of the páramo during or after the ash deposit episodes. This zone provides evidence for high moisture and warm temperatures on the páramo.

Pollen Zone P7, 141-74 cm, 770 - 325 cal yr BP, 25 samples, 18 years / sample

With two tephra layers, M2, which ended at the beginning of zone 7 (130 cm), and M1, which ended at 115-110 cm (1600 AD), zone 7 was characterized by the disappearence of *Ambrosia* (3,5-0%), an increase in *Gentianella* (1-12%), Poaceae (17-36%) and Ast liguliflorae (from 1-7% to 15-25% at the end of the zone). The convective activity index decreased abruptly at the beginning of the zone with the decrease in *Alnus* and *Hedyosmum* up to 105 cm when it again started to increase. A 11-35% peak in Urticales occurred at 122-112 cm. Charcoal particle abundance remained low with a peak at the end of zone P7. This zone shows drier conditions than the previous zone. Burned biomass was low and no fire events were detected.

Pollen Zone P8, 74-0 cm, 325 -0 cal yr BP, 29 samples, resolution 3 years / sample

No tephra deposition occurred in the sediment in the last 340 years. Zone 8 was characterized by an increase in Apiaceae and *Ambrosia* (2-11%), the highest convective index of the record (0.25), the absence of charcoal particles except for a peak in the last decade, high *Huperzia* frequency (19-405%), a sharp decrease in Poaceae (from 30 to 8%), a 10-22% increase followed by a 22-1% decrease in Apiaceae throughout the zone. High convective activity and low soil moisture characterized the hydrological pattern of this zone. Burned biomass was low and only one fire event was detected.

For a detailed description of the last 700 years, i.e. 1300 AD to 2008 AD, see Ledru et al. (2013).

Interpretation and Discussion

To analyze how the forcing factors, climate, fire and tephra deposition, alternately influenced the landscape of the páramo, we compared the convective activity index with published palaeoclimate records that are representative of ENSO variability and SASM activity (Figs. 1A, 6). ENSO variability refers to the changes in equatorial Pacific Sea Surface Temperature (SST) that impacted high elevation rainfall variability at interdecadal scales (Morales et al., 2012; Garreaud et al., 2009; Ledru et al., 2013). To characterize El Niño activity, we used the record of El Junco in the Galapagos where blooms of the algae *Botryococcus* that are associated with high rainfall recorded weak El Niño activity until 3500 cal yr BP (Fig. 6) (Zhang et al., 2014). Further south, at Guayaquil, Uk′37-based SST changes were reconstructed from a marine core and revealed several fluctuations in SST during the early and mid-Holocene until 2500 yr BP when the ITCZ reached the latitude of Guayaquil (Mollier-Vogel et al., 2013;

Seillès et al., 2015). SASM activity at pluridecadal scale was characterized by changes in the oxygen isotope ratio measured in speleothems located in the Eastern Cordillera. Both Shatuca (1960 m asl) and Huagapo (further south at 3850 m asl) records show a synchronous decrease in moisture along the EC until 2500 yr BP (Bustamante et al., 2013; Kanner et al., 2013). After this date, an out-of-phase evolution can be observed between the records (Fig. 6), suggesting that the increase in ENSO activity is well detected at high elevations while at Shatuca, the SASM forcing became dominant after 2500 yr BP.

At Papallacta, two main increases in the convective index reflecting higher monsoon activity occurred at ~2500 BP and at 400 BP while the lowest values of the index occurred at 2600, 1200 and 600 cal yr BP (Fig. 6). *Polylepis* pollen is permanently present in the area of Papallacta, with some peaks in the bottom of the core followed by full expansion from 3500 cal yr BP until today (Fig. 4).

Fires and tephra deposition

Although the páramo has been present at the elevation of Papallacta for the last 5,000 years (Di Pasquale et al., 2008), some changes in its floristic assemblages, e.g., shifts from Poaceae dominant páramo to Asteraceae dominant páramo, suggest high sensitivity either to climate or other disturbances such as fire or tephra deposition. Today in the páramo, frequent burning can be either natural, or linked to volcanic or human activities (Horn and Kapelle, 2009). Fires do not appear to have been a common disturbance at Papallacta in the last 5,000 years as only four major episodes can be distinguished. Charcoal peaks may appear at Papallacta due to the long-distance transport of charcoal particles from volcanic eruptions and the associated increase in dry and highly flammable fuels due to tephra-induced plant mortality (Horn and Kapelle, 2009). Thus, when charcoal abundances increased shortly after a tephra deposition, we infer a potentially tephra-induced fire event occurred. Soil moisture is characterized by the frequency of Poaceae pollen (Ledru et al., 2013) and changes can be caused either by climate or tephra deposition (Horn and Kapelle, 2009). Three abrupt changes in soil moisture content evidenced by drops in Poaceae pollen percentages can be seen in Figs. 3 and 4. The first drop (from 53% to 6%) at ~4700 cal BP follows the 10-cm-thick M18 tephra deposition and is associated with higher quantities of burned biomass and low FRI values (Fig. 5). Thus, in a scenario where tephra deposition enhances soil and fuel drought, the Poaceae drop could have been triggered by fires. This event lasted for 260 years and the vegetation took 60 years to fully recover. Due to the relatively long duration of this drier event (260 years), we infer that, during this interval, a volcanic effect on the soil was coupled with dry climate conditions. Although of less amplitude than the ones described above, another fire event at 4100 cal yr BP associated with a drop in Poaceae could result from the effect of the M16 tephra deposition.

The second drop in the frequency of Poaceae pollen occurred between 3450 and 2900 cal yr BP. No tephra deposition was observed during this event but the FRI was low (50 yr at ~3100 yr BP). When FRI increased again, the recovery of the vegetation lasted less than 50 years and was chararcterized by the expansion of two taxa, which, according to our modern survey, are indicators of drier and cooler climate conditions, Apiaceae and Asteraceae liguliflorae (Ledru et al, 2013). The third drop in Poaceae

pollen frequency occurred between 2600 and 2400 cal yr BP right after the M11 tephra deposition and at the same time as a fire fueled by Poaceae observed at the beginning of this episode (Fig. 5).

Between 1800 and 770 cal yr BP, the synchronous increase in the concentration of charcoal particles, *Ambrosia* pollen, cloud forest tree taxa and bog taxa *Huperzia* (Fig. 4, 5) suggests high moisture and warm conditions and characterizes the warmest interval of the pollen record. Under such moist and warm climate conditions, the low FRI is probably related to increased human activity, which reached higher elevations during this interval with minor fluctuations recorded at 1750, 1550 and around 900 cal yr BP. The same conclusion was inferred at Lake La Cocha (González-Carranza et al., 2012).

Between 770 and 325 cal yr BP, the simultaneous disappearance of *Ambrosia*, Apiaceae pollen and cloud forest tree taxa, and the expansion of Ast. *Senecio* suggests drier soil and atmospheric conditions than in the previous interval. This is the driest interval of the pollen record which, due to its long duration, could result from both tephra deposition (M2 layer) and climate conditions (Ledru et al., 2013).

During the last century, between 250 and 150 cal yr, the expansion of the Apiaceae pollen percentages, the re-expansion of *Ambrosia* and cloud forest tree taxa and the high *Huperzia* frequency suggest high moisture rates on the paramo.

Out of seven changes in the landscape, we attribute two to tephra deposition (4100 and 2550 cal yr BP), two of longer duration are associated with the superimposed effect of tephra deposition and climate change (respectively 4600-4440 cal yr BP and 770-325 cal yr BP), two events are exclusively attributed to climate change (3450-2900 cal yr BP and 250-150 cal yr BP) and one to human activity between 1800 and 770 cal yr BP. In the following section, we discuss the climate patterns.

Climate forcings, SASM versus El Niño activity

The bog at the base of core PA1-08 was not fully expanded, probably due to vegetation recovery after the deposit of two meters of organic mud and reworked tephra. However, high Poaceae and cloud forest tree taxa frequencies suggest a high moisture level at Papallacta at the beginning of the record.

The pollen record of the last 1,000 years showed statistically significant vegetation changes (pollen zones P-6 to P-8; Fig. 4), including fluctutations of transported tree pollen, *Ambrosia*, and Apiaceae frequencies, that were broadly synchronous with Sea Surface Temperature changes during the Medieval Climate Anomaly (MCA) and the Little Ice Age (LIA) (Ledru et al., 2013). An intermediate dry period, characterized by low tree frequencies and the regression of *Ambrosia* between the MCA and the LIA (zone P-7), also identified by Apaéstegui et al. (2018), highlights the response of páramo biodiversity under both low ENSO variability and low convective activity. Thus, the pollen record spanning the last 1000 years shows how the two sources of moisture, namely the year-round adiabatic cloud dripping linked to SASM activity and the ENSO variability at decadal scale, influenced the vegetation cover around Papallacta. Here our aim was to understand how these moisture sources behaved during the late Holocene with an additional driver represented by summer insolation and including the regional volcanic activity with 18 tephras deposited over the course of the last 5,000 years.

At millennial scale, the progressive increase in convective moisture mirrors the long-term trend toward more intense SASM driven by higher austral summer insolation in agreement with other records (e.g., Seillès et al., 2015). The increase in insolation drove a progressive increase in adiabatic moisture to higher elevation that today represents its highest index in the last 5,000 years (Fig. 6).

The first interval, between 5000 and 2450 cal yr BP, was characterized by high soil moisture, low adiabatic moisture and four increases in the number of charcoal particles associated with fire events (Fig. 4 and 5). The abrupt changes in environmental conditions that occurred between 4600 and 4475 cal yr BP (corresponding to pollen zone 2) lasted 150 years and were associated with less adiabatic moisture along the eastern cordillera and low rainfall on the páramo, in agreement with the weakening of the SASM in the Amazon basin and the low frequency of El Niño on the Pacific side (Bustamante et al., 2013; Zhang et al., 2014). The northernmost position of the ITCZ and the weaker SASM activity (Maksic et al., 2019) also resulted in drier climate conditions further east, in northeastern Brazil (Montade et al., 2014; Utida et al., 2020), thus confirming similar responses to climate changes by the high tropical Andes and Northeastern Brazil and possible links between the two regions (Vuille et al., 1999; Mollier-Vogel et al., 2013; Sulca et al., 2016). Another simulation showed that during this interval, northern Ecuador was under the influence of the northern hemisphere cooling but does not exclude the possibility of cooling caused by a huge volcanic eruption (Ning et al., 2019).

Between 3450 and 2900 cal yr BP, the dry soil conditions, the increase in adiabatic moisture and the cooler temperature are consistent with the lacustrine record of Pallcacocha in Peru (4200 m asl) (Moy et al., 2002) as well as with the speleothem records, Tigre Perdido (1000 m asl), Shatuca (1960 m asl) and Huagapo (3850 m asl) (Fig. 6). This period of increased humidity in the Amazon basin was interpreted as changing SST gradients in the tropical Atlantic (Bustamante et al., 2016; van Beukelen et al., 2008; Kanner et al., 2013). At the same time, ~3500 to 2600 cal yr BP, El Niño became both more frequent and more intense (Fig. 6) and, near the Ecuadorian coast area, the interval between 4200 and 2850 cal yr BP was marked by the coolest and driest climate conditions of the Holocene, due to the weak influence of the ITCZ and strengthening of the Humboldt Current in the Pacific Ocean (Fig.1A) (Seillès et al., 2015). Thus, our results show that the increase in El Niño frequency was superimposed on the strengthening of the Humboldt Current able to maintain drier conditions on the paramó, thus hampering the high monsoon activity recorded in the Amazon basin.

The progressive uplift in adiabatic moisture and in the upper forest limit started after 2450 cal yr BP and was characterized by an abrupt change in Poaceae and fire activity on the paramo (Fig. 4, 5). On the Pacific side, the date of ~2500 cal yr BP marks the time when the ITCZ reached the latitude of Papallacta and the beginning of the bimodal precipitation regime observed today along the coast (Mollier-Vogel et al., 2013). At higher elevations, this bimodal regime is hampered by permanent moisture originating from the Amazon basin, also related to the southern shift of the ITCZ and SASM activity, which is superimposed on moisture linked to the Pacific-SST. Within these two intervals separated by 2450 cal

yr BP and superimposed on the long-term influence of insolation on the Andean records, centennial- or multidecadal-scale environmental changes occurred at Papallacta and are described below (Fig. 6).

During the second interval of the record, between 2450 and 0 cal yr BP, lower Poaceae frequencies (~30%), there was no - or only weak - fire activity (Fig. 4, 5). In addition, the progressive increase in the convective index (Fig. 5) suggests upslope expansion of the upper forest limit synchronous with a southward shift of the the ITCZ (Seillès et al., 2015) and enhanced SASM on the Amazon side, as also reported at Lake La Cocha (2,780 m asl) near Papallacta (González-Carranza et al., 2012; van Boxel et al., 2014). From 2300 to 1900 cal yr BP, drier soil conditions and colder temperatures were followed by a warmer episode that lasted until 1550 cal yr BP, synchronous with an increase in ENSO activity between 2000 and 1500 cal yr BP (Rein et al., 2005; Zhang et al., 2014). Changes in the convective index point to two drier episodes at 2550 and 1300 cal yr BP (Fig 6). At about 500 km south of Papallacta and at 3,800 m asl, two drier episods, between 2700 and 2000 cal yr BP and between 1700 and 1000 cal yr BP, were also observed in the lacustrine record of Tres Lagunas (Frederick et al., 2018) and can be attributed to abrupt changes in SASM activity at centennial scale.

Modern-day El Niño conditions are characterized by a weaker monsoon and reduced transport of moisture and warmer temperatures on the páramo with the reverse situation under La Niña conditions (Garreaud, 2009). The wet climate episodes observed at Papallacta before 2450 cal yr BP and in the last 500 years were both characterized by low El Niño frequency while the dry episode with low soil moisture between 2450 and 1300 cal yr BP was characterized by high El Niño frequency between 2400 and 2000 cal yr BP and low El Niño frequency after 2000 cal yr BP (Zhang et al., 2014) (Fig. 6). Between 1500 and 1000 cal yr BP, the low El Niño frequency (Fig. 6) probably impacted the SASM activity as a marked decrease in adiabatic moisture was observed at Papallacta during this interval (Vuille et al 2000). High SASM activity (high convective index) was observed up to the elevation of Papallacta at 4600 cal yr BP, 4400 cal yr BP, between 2400 and 1500 cal yr BP and during the last 500 years, while low SASM activity (low convective index) was observed at ~4550, 2550, 1200 and 700 cal yr BP (Fig. 6).

Thus, our results show that the influences of the long-term insolation (precession-scale) forcing and of the multi-century fluctuations in SASM activity on precipitation over the high summits of the Andes are stronger than the influence of ENSO variability at multi-centennial to multi-decadal scales. Differences in the intensity and/or amplitude of the signal are also observed between the Andean records emphasizing the considerable spatial variability associated with SASM activity. For instance, at Shatuca and Tigre Perdido, the long dry period that lasted ~200 years at about 2300 cal yr BP (Bustamante et al., 2016; van Breukelen et al., 2008) does not correspond to the driest period at Papallacta. The multi-decadal changes observed in the speleothem records, for instance, the increase in moisture between 3500 and 2900 cal yr BP, are not observed at Papallacta or in the lacustrine record of Tres Lagunas (Frederick et al., 2018), suggesting that the vegetation was not impacted and/or that the amplitude of the event was smaller at higher elevations. The influence of the intensity of the SASM on precipitation variability over

the high summits of the Andes after 2500 yr BP is also visible in the Ti/Ca sediment record of Mollier-Vogel et al. (2013) from the Gulf of Guayaquil (4°S) (Fig. 6). However, during the late Holocene, at both low and high elevations, the influence of the precession cycle on the gradual increase in moisture was punctuated by centennial-scale deviations, indicating other influences triggered the considerable spatial variability associated with the SASM (Kanner et al.2013; Vuille and Werner, 2005).

Conclusion

Our results show that the páramo is a very sensitive ecosystem to long-term insolation and to the series of multi-centennial to multi-decadal-scale events in the late Holocene. We found two types of responses of the vegetation cover depending on the origin of the moisture: soil with the expansion/regression of Poaceae / Ast. *Senecio,* and atmospheric moisture with cloud dripping enhanced by the adiabatic upslope between the Amazon basin and the high summits of the Eastern Cordillera. During the last 5,000 years, the Andean forest upper limit never reached the elevation of the Sucus bog at Papallacta and the 18 regional tephra fallout deposits had almost no impact on the biodiversity of the páramo, only on the local drainage of the bog. However, in the long term, at precession scale, and superimposed on the short term, multi-centenial to multi-decadal climate events strongly modified the floristic composition of the páramo with frequent fires before 2450 cal yr BP. The driest event in the last 5,000 years characterized by the lowest convective index occurred at ~4500 cal yr BP, when both mean annual precipitation decreased and convective moisture abruptly stopped reaching the elevation of Papallacta. In the last century, the adiabatic moisture upslope reached its strongest amplitude. By comparing our results with marine, speleothem, lake or bog records, we also emphasize how in the Tropics, a single climate event may be manifest in a wide range of effects depending on the elevation and location of the site, confirming the influence of the SASM on precipitation variability over the high summits of the Andes.

Acknowledgements

Radiocarbon dates were measured at the *Laboratoire de Mesure du Carbone 14* (LMC14) – UMS 2572 (CEA/DSM CNRS IRD IRSN). We thank the *Ministerio del Ambiente del Ecuador* for permitting and facilitating our fieldwork at Papallacta, the INAMHI for providing climate data, Katerine Escobar-Torrez for help with the figures in an earlier version, Marjorie Herrera, Boromir Bogumil and Jörg Bogumil for coring and fieldwork in 2009, Benjamin Bernard, Marco Córdova and Edwin Telenchana for coring in 2014.

Funding

This research was funded by UR GREAT ICE (IRD) and UMR ISEM (Univ. of Montpellier, CNRS, IRD, EPHE).

References

Apaéstegui J, Cruz FW, Vuille M et al. (2018) Precipitation changes over the eastern Bolivian Andes inferred from speleothem (δ18O) records for the last 1400 years. *Earth and Planetary Science Letters* 494: 124-134.

Bakker J, Moscol-Olivera M and Hooghiemstra H (2008) Holocene environmental change at the upper forest line in northern Ecuador. *The Holocene* 18: 877–893.

Bendix J, Rollenbeck R and Reudenbach C (2006a) Diurnal patterns of rainfall in a tropical Andean valley of southern Ecuador as seen by a vertically pointing K-band Doppler radar. *International Journal of Climatology* 26: 829-846.

Bendix J, Rollenbeck R, Göttlicher D and Cermak J (2006b) Cloud occurrence and cloud properties in Ecuador. *Climate Research* 30: 133-147.

Bendix J, Homeier J, Cueva Ortiz E et al. (2006c) Seasonality of weather and tree phenology in a tropical evergreen mountain rain forest. *International Journal Biometeorology* 50: 370-384.

Bennett KD (1996) Determination of the number of zones in a biostratigraphical sequence. *New Phytologist* 132: 155–170.

Bennett KD (2008) *Psimpoll v. 4.26*. Available at: http://chrono.qub.ac.uk/psimpoll/psimpoll.html.

Birks HJB and Gordon AD (1985) *Numerical Methods in Quaternary Pollen Analysis*. London: Academic Press.

Blaauw M, Christen AJ, Aquino Lopez MA (2021) Rbacon: age-depth modelling using bayesian statistics. R package version 2.5.6. https://CRAN.R-project.org/package=rbacon

Borrelli P, Armenteras D, Panagos P et al. (2015) The implications of fire management in the andean páramo: A preliminary assessment using satellite remote sensing. *Remote Sensing* 7: 11061-11082.

Bustamante MG, Cruz FW, Vuille M et al. (2016) Holocene changes in monsoon precipitation in the Andes of NE Peru based on $\delta^{18}O$ speleothem records. *Quaternary Science Reviews 146: 274-287.*

Buytaert W, Célleri R, De Bièvre C et al. (2006) Human Impact on the hydrology of the Andean Páramos. *Earth-Science Reviews* 79: 53-72.

Caceres B, Francou B, Favier V et al. (2006) Glacier 15, Antisana, Ecuador: its glaciology and relations to water resources. IAHS, *Climate Variability and Change - Hydrological Impacts* 308: 479-482.

Clapperton CM, Hall M, Mothes P et al. (1997) A Younger Dryas Icecap in the Equatorial Andes Quaternary Research 47: 13–28.

Conroy JL, Restrepo A, Overpeck, JT et al. (2009) Unprecedented recent warming of surface temperatures in the eastern tropical Pacific Ocean. *Nature Geosciences* 2 : 46–50.

Cour P (1974) Nouvelle techniques de détection des flux et des retombées polliniques: Etude de la édimentation des pollens et des spores à la surface du sol. *Pollen et Spores* XVI : 103-141.

Courtney-Mustaphi CJ, Pisaric MFJ (2014) A classification for macroscopic charcoal morphologies found in Holocene lacustrine sediments. *Progress in Physical Geography: Earth and Environment* 38:734-754. https://doi.org/10.1177/0309133314548886

Di Pasquale G, Marziano M, Impagliazzo S, et al. (2007) The Holocene treeline in the Northern Andes (Ecuador): First evidence from soil charcoal. *Palaeogeography, Palaeoclimatology, Palaeoecology* 259: 17– 34.

Enache MD, Cumming BF (2006) Tracking recorded fires using charcoal morphology from the sedimentary sequence of Prosser Lake, British Columbia (Canada). *Quaternary Research* 65: 282-292.

Faegri, K. and Iversen, J.: Textbook of pollen analysis, 4 Edn., J.Wiley & Sons, Chichester, UK, 1989.

Feurdean A (2021) Experimental production of charcoal morphologies to discriminate fuel source and fire type: an example from Siberian taiga. *Biogeosciences* 18:3805–3821. https://doi.org/10.5194/bg-18-3805-2021

Finsinger W, Kelly R, Fevre J and Magyari EK (2014) A guide to screening charcoal peaks in macrocharcoal-area records for fire-episodes reconstructions. *The Holocene* 24: 1002–1008.

Finsinger W, Magyari EK, Fevre J et al. (2016) Holocene fire regimes near the treeline in the Retezat Mts (Southern Carpathians). *Quaternary International* 477: 94-105.

Flantua SGA, O'Dea A, Onstein RE et al. (2019) The flickering connectivity system of the north Andean páramos. *Journal of Biogeography* 46:1808-1825.

Frederick L, Brunelle A, Morrison M et al. (2018) Reconstruction of the mid-Holocene paleoclimate of the Ecuadorian Andean páramo at Tres Lagunas, Ecuador. *The Holocene* 28: 1131-1140.

Garreaud RD (2009) The Andes climate and weather. *Advances in Geosciences* 22: 3-11.

Garreaud RD, Vuille M, Compagnucci R et al. (2009) Present-day South American climate. *Palaeogeography Palaeoclimatology Palaeoecology* 281: 180–195.

González-Carranza Z, Hooghiemstra H, Vélez MI (2012) Major altitudinal shifts in Andean vegetation on the Amazonian flank show temporary loss of biota in the Holocene. *The Holocene* 22:1227-1241.

Grubb PJ, Lloyd R, Pennington TD, Páez-Bimos S (2020) A historical baseline study of the páramo of Antisana in the Ecuadorian Andes including the impacts of burning, grazing and trampling. *Plant Ecology & Diversity* 13: 225-256.

Hall ML, Mothes PA, Samaniego P, Militzer A, Beate B, Ramón P, Robin C (2017) Antisana volcano: A representative andesitic volcano of the eastern cordillera of Ecuador: Petrography, chemistry, tephra and glacial stratigraphy. *Journal of South American Earth Sciences* 73: 50-64.

Hastenrath S (1981) The Glaciation of the Ecuadorian Andes. CRC Press.

Haug GH, Hughen KA, Sigman DM et al. (2001) Southward migration of the intertropical convergence zone through the Holocene. *Science* 293: 1304–1306.

Herrera M (2010) Polen y esporas del Bosque de Papallacta, Biologia, Universidad Centrale del Ecuador (UCE), Quito, 120 pp.

Higuera PE, Brubaker LB, Anderson PM et al. (2009) Vegetation mediated the impacts of postglacial climate change on fire regimes in the south-central Brooks Range, Alaska. *Ecological Monographs* 79: 201-219.

Higuera PE, Gavin DG, Bartlein PJ et al. (2010) Peak detection in sediment–charcoal records: impacts of alternative data analysis methods on fire-history interpretations. *International Journal of Wildland Fire* 19: 996. https://doi.org/10.1071/WF09134

Hooghiemstra H (1984) Vegetational and climatic history of the high plain of Bogotá, Colombia: A continuous record of the last 3.5 million years, J. Cramer, Vaduz.

Hooghiemstra H and Flantua SGA (2019) Colombia in the Quaternary: An overview of environmental and climatic change. In: Góme J and Pinilla–Pachon AO (eds) *The Geology of Colombia* vol. 4. Bogotá: Servicio Geológico Colombiano, Publicaciones Geológicas Especiales, pp. 38-52.

Hogg AG, Heaton TJ, Hua Q et al. (2020) SHCal20 Southern Hemisphere Calibration, 0–55,000 Years cal BP. *Radiocarbon*. 62: 759–778.

Horn SP and Kappelle M (2009) Fire in the páramo ecosystems of Central and South America. In: Cochrane MA (ed) *Tropical fire ecology*. Berlin: Springer, pp.505-539.

Jansen B, de Boer EJ, Cleef AM et al. (2013) Reconstruction of late Holocene forest dynamics in northern Ecuador from biomarkers and pollen in soil cores *Palaeogeography Palaeoclimatology Palaeoecology* 386: 607–619.

Jensen K, Lynch EA, Calcote R et al. (2007) Interpretation of charcoal morphotypes in sediments from Ferry Lake, Wisconsin, USA: do different plant fuel sources produce distinctive charcoal morphotypes? *The Holocene* 17: 907-915.

Jorgensen PM and Leon-Yanez S (1999) Catalogue of the vascular plants of Ecuador, Missouri Botanical Garden, Saint Louis Missouri USA.

Juggins S (2015) Rioja: Analysis of Quaternary Science Data, R package version (0.9-9). (http://cran.r-project.org/package=rioja)

Kanner LC, Burns SJ, Cheng H et al. (2013) High-resolution variability of the South American summer monsoon over the last seven millennia: insights from a speleothem record from the central Peruvian Andes. *Quaternary Science Reviews* 75: 1-10.

Kaufman D, McKay N, Routson C et al. (2020). A global database of Holocene paleotemperature records. *Scientific Data* 7**:** 115 https://doi.org/10.1038/s41597-020-0445-3

Kelly R, Higuera PE, Barrett CM, Hu FS (2011) A signal-to-noise index to quantify the potential for peak detection in sediment–charcoal records. *Quaternary Research* 75:11–17. https://doi.org/10.1016/j.yqres.2010.07.011

Körner C and Paulsen J (2004) A world-wide study of high altitude treeline temperatures. *Journal of Biogeography* 31: 713-732.

Kuentz A (2009) Dynamiques actuelle et holocène de la puna (Andes sèches du Pérou) à partir des observations de terrain, de la cartographie (SIG) et de la palynologie (région du Nevado Coropuna), Université Blaise Pascal, Clermont-Ferrand, 256 pp.

Ledru MP, Jomelli V, Samaniego et al. (2013) The Medieval Climate Anomaly and the Little Ice Age in the Eastern Ecuadorian Andes. *Climate of the Past* 9: 307-321.

Liu K-B, Reese CA, Thompson LG (2005) Ice-core pollen record of climatic changes in the central Andes during the last 400 yr. *Quaternary Research* 64: 272–278.

Luteyn J (1999) Páramos: A Checklist of Plant Diversity, Geographical Distribution, and Botanical Literature (Memoirs of the New York Botanical Garden, vol. 84). The New York Botanical Garden Press, New York.

Maksic J, Shimizu MH, Sampaio de OG et al 2019 Simulation of the Holocene climate over South America and impacts on the vegetation. *The Holocene* 29: 287-299.

Marengo JA (2009) Long-term trends and cycles in the hydrometeorology of the Amazon basin since the late 1920's. *Hydrol. Process* 23, 3236–3244.

Marengo JA and Nobre CA (2001) General characteristics and variability of climate in the Amazon basin and its links to the global climate system. In: Mcclain ME, Victoria RL and Richey JE (eds)*The biogeochemistry of the Amazon Basin*, Oxford University Press.

Marlon JR, Bartlein PJ, Carcaillet C et al. (2008) Climate and human influences on global biomass burning over the past two millennia. *Nature Geosciences* 1:697–702. https://doi.org/10.1038/ngeo313

Matson E and Bart D (2013) Interactions among fire legacies, grazing and topography predict shrub encroachment in post-agricultural paramo. *Landsc Ecol* 28:1829–1840 doi: 10.1007/s10980-013-9926-5

Moy CM, Seltzer GO, Rodbell DT et al. (2002) Variability of El Nino/Southern Oscillation activity at millennial time scales during the Holocene epoch. *Nature* 420: 162-165.

Mollier-Vogel E, Leduc G, Böschen T et al. (2013) Rainfall response to orbital and millennial forcing in northern Peru over the last 18 ka. *Quaternary Science Reviews* 76: 29-38.

Montade V, Ledru MP, Burte J et al. (2014) Stability of a Neotropical microrefugium during climatic instability. *J. Biogeogr.* 41: 1215e1226.

Morales MS, Christie DA, Villalba R et al. (2012) Precipitation changes in the South American Altiplano since 1300 AD reconstructed by tree-rings. *Clim. Past* 8: 653-666.

Moscol Olivera M, Duivenvoorden JF and Hooghiemstra H (2009) Pollen rain and pollen representation across a forest-páramo ecotone in northern Ecuador. *Review of Palaeobotany and Palynology* 157: 285-300.

Moscol Olivera MC and Hooghiemstra H (2010) Three millennia upper forest line changes in northern Ecuador: pollen records and altitudinal vegetation distributions. *Review of Palaeobotany and Palynology* 163: 113–126.

Ning L, Liu J, Bradley RS, Yan M (2019) Comparing the spatial patterns of climate change in the 9th and 5th millennia BP from TRACE-21 model simulations. *Climate of the Past* 15: 41–52.

Ortuño T (2008) Relation végétation pollen climat dans les écorégions de Bolivie. Master FENEC, University of Montpellier, France, 45 pp.

Prado LF, Wainer I, Chiessi CM et al. (2013) A mid-Holocene climate reconstruction for Eastern South America. *Climate of the Past* 9: 2117-2133.

Ramsay PM and Oxley ERB (1997) The growth form composition of plant communities in the Ecuadorian páramos. *Plant Ecology*131: 173-192

Rein B, Lückge A, Reinhardt L et al. (2005) El Niño variability off Peru during the last 20,000 years. *Paleoceanography* 20 : PA4003.

Rhodes AN (1998) A method for the preparation and quantification of microscopic charcoal from terrestrial and lacustrine sediment cores. *The Holocene* 8: 113-117.

Rodbell DT, Seltzer GO, Anderson DM et al. (1999) A 15, 000 year record of El-Niño driven alluviation in southwestern Ecuador. *Science* 283: 516–520.

Sarmiento FO and Frolich LM (2002) Andean cloud forest tree lines: naturalness, agriculture and the human dimension. *Mountain Research and Development* 22: 278-287.

Schlachter KJ and Horn SP (2010) Sample preparation methods and replicability in macroscopic charcoal analysis. *Journal of Paleolimnology* 44: 701-708.

Segura H, Junquas C, Espinoza JC et al. (2019) New insights into the rainfall variability in the tropical Andes on seasonal and interannual time scales *Climate Dynamics* 53: 405-426.

Seillès B, Sánchez Goñi MF, Ledru M-P et al. (2015) Holocene land–sea climatic links on the equatorial Pacific coast (Bay of Guayaquil, Ecuador). *The Holocene* 26: 567-577.

Sklenar P and Jorgensen PM (1999) Distribution patterns of páramo plants in Ecuador. *Journal of Biogeography* 26: 681-691.

Sulca J, Vuille M, Silva Y, Takahashi K (2016) Teleconnections between the Peruvian Central Andes and Northeast Brazil during Extreme Rainfall Events in Austral Summer. *Journal of Hydrometeorology* 17: 499–515

Tejedor E, Steiger NJ, Smerdon JE et al. (2021) Global hydroclimatic response to tropical volcanic eruptions over the last millennium. *Proceedings of the National Academy of Sciences* 118: e2019145118;

Turney CSM and Lowe JJ (2001) Tephrochronolgy. *Tracking Environmental Change Using Lake Sediments*. Dordrecht, The Netherlands: Kluwer Academic Publishers, 451–471

Urrutia R and Vuille M (2009) Climate change projections for the tropical Andes using a regional climate model: Temperature and precipitation simulations for the end of the 21st century. *J. Geophys. Res. Atmos. Atmos.* 114: D02108. doi: 10.1029/2008JD011021.

Utida G, Cruz FW, Santos RV et al. (2020) Climate changes in Northeastern Brazil from deglacial to Meghalayan periods and related environmental impacts. Quaternary Science Reviews 250, 106655

Valencia BG, Bush MB, Coe AL et al. (2018) Polylepis woodland dynamics during the last 20,000 years. Journal of Biogeography 45: 1019–1030. https://doi.org/10.1111/jbi.13209

van Boxel JH, González-Carranza Z, Hooghiemstra H et al. (2014) Reconstructing past precipitation from lake levels and inverse modelling for Andean Lake La Cocha. *Journal of Paleolimnology* 51: 63-77.

van Breukelen MR, Vonhof HB, Hellstrom JC et al. (2008) Fossil dripwater in stalagmites reveals Holocene temperature and rainfall variation in Amazonia. *Earth and Planetary Science Letters* 275: 54-60.

Vuille M, Bradley RS, Keimig, F (2000) Climatic variability in the Andes of Ecuador and its relation to tropical Pacific and Atlantic sea surface temperature anomalies. *J. Climate* 13: 2520–2535,

Vuille M and Werner M (2005) Stable isotopes in precipitation recording South American summer monsoon and ENSO variability – observations and model results. *Climate Dynamics* 25: 401–413.

Whitlock C and Larsen C (2001) Charcoal as a fire proxy. In: Smol JP, Birks HJB, Last WM (eds.) *Tracking Environmental Change Using Lake Sediments: Terrestrial, Algal, and Siliceous Indicators,* vol. 3. Dordrecht: Kluwer Academic Publishers, pp. 75-97.

Zúñiga-Escobar O, Uribe A, Torres-González AM et al. (2013) Assessment of the impact of anthropic activities on carbon storage in soils of high montane ecosystems in Colombia. *Agronomía Colombiana* 31: 112-119.

Zhang Z, Leduc G and Sachs JP (2014) El Niño evolution during the Holocene revealed by a biomarker rain gauge in the Galápagos Islands. *Earth and Planetary Science Letters* 404: 420-434.

List of tables

Table 1 Description of the vegetation cover around Papallacta bog (from Ledru et al., 2013).

Table 2 Chronology of core PA1-08. Radiocarbon ages measured on total organic matter from sediments in the PA1-08 core.

Table 3 Description of the tephra layers in PA1-08 shown in Fig. 3 with the origin and the year of the eruption re-calculated from our age model (see also supplementary Tables S1 and S2). WC Western Cordillera, EC Eastern Cordillera.

Figures with Figure captions

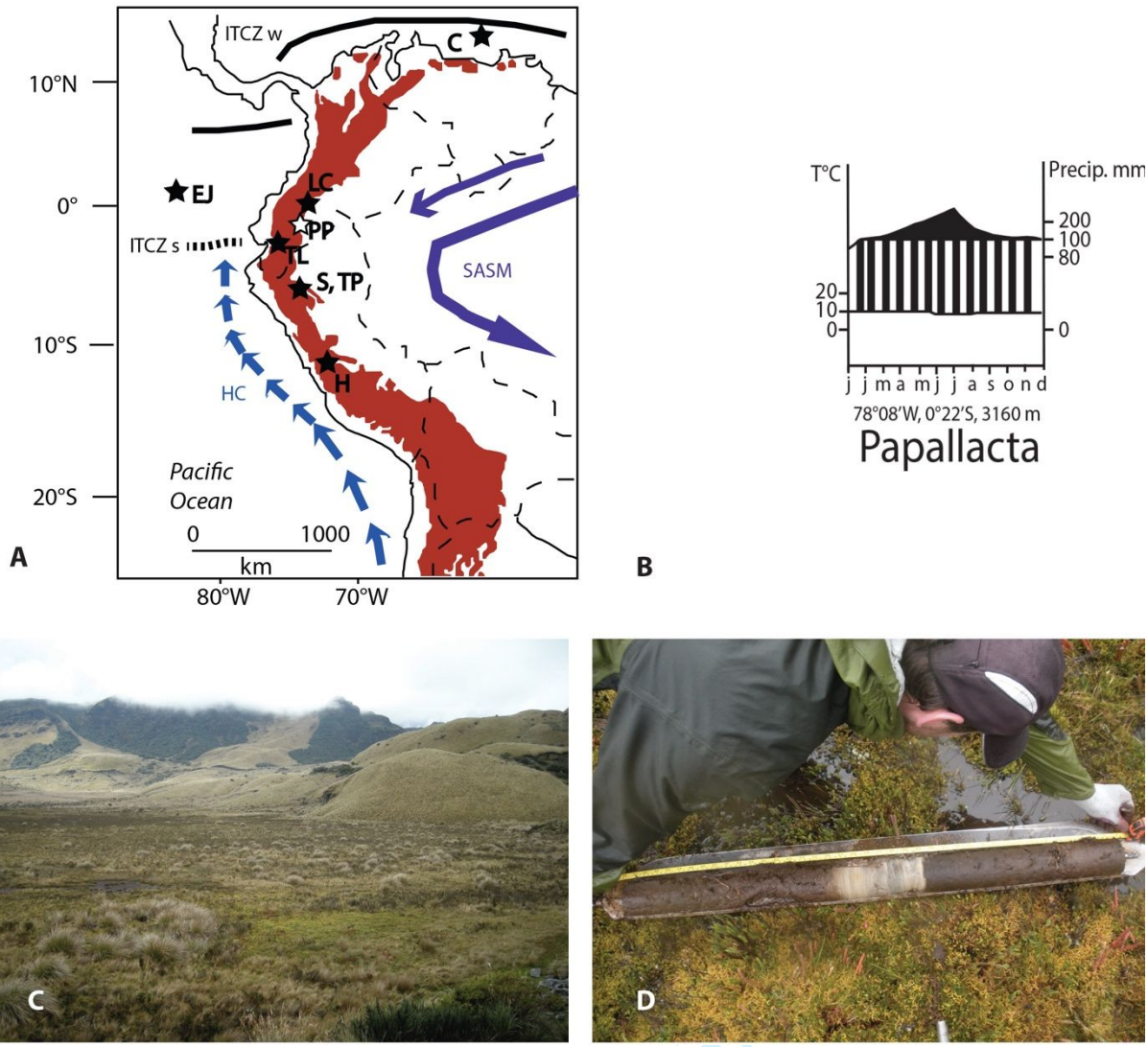

Figure 1: A) Map of western South America showing the tropical Andes (in red), the location of Papallacta bog (white star), the location of some of the records cited in the text (C Cariaco (Haug et al., 2001), LC Lake La Cocha (González-Carranza et al., 2012), TL Tres Laguna (Frederick et al., 2018), S Shatuca (Bustamante et al., 2016), TP Tigre Perdido (van Breukelen et al., 2008), H Huagapo (Kanner et al., 2013)) and the main climatic features discussed in the text (ITCZw is the position of the InterTropical Convergence Zone in winter, ITCZs in summer, HC the Humboldt Current, SASM South American Summer Monsoon). B) Climate information represented on a Walter diagram (Luteyn, 1999). Temperature is shown by the bottom curve, precipitation by the upper curve. C) The bog at Papallacta with patches of *Polylepis* forest on the background slopes. D) View of the M2 tephra in core PA1-08 (©MP Ledru)

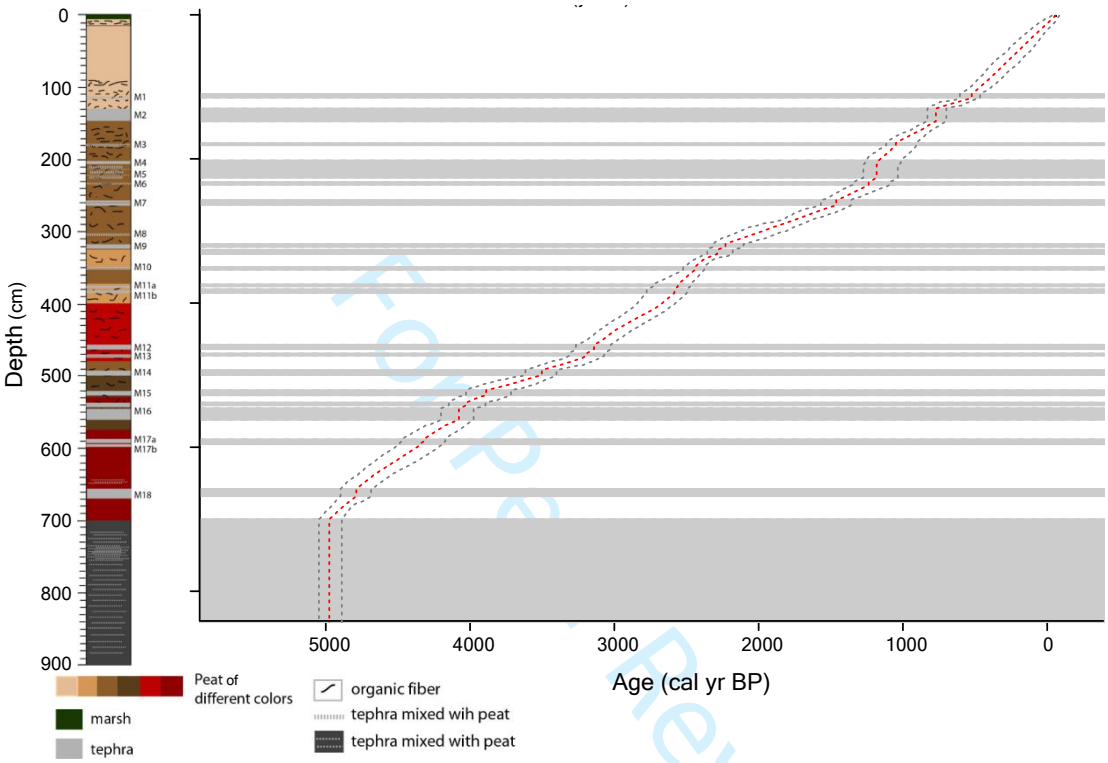

Figure 2: Lithology of the PA1-08 core of Papallacta showing the location of tephra layers M1 to M18 (see Table 3). Grey rectangles along the depth scale indicate the thickness of the tephra layers. Bacon age/depth model of core PA1-08 (red dashed line) overlaying the calibrated distributions of the individual radiocarbon dates (blue) (see Table 2) and the age of the tephra deposits (in green) reported in Table 3. Dark grey areas show the 95% confidence intervals of the models (Blaauw and Christen, 2011).

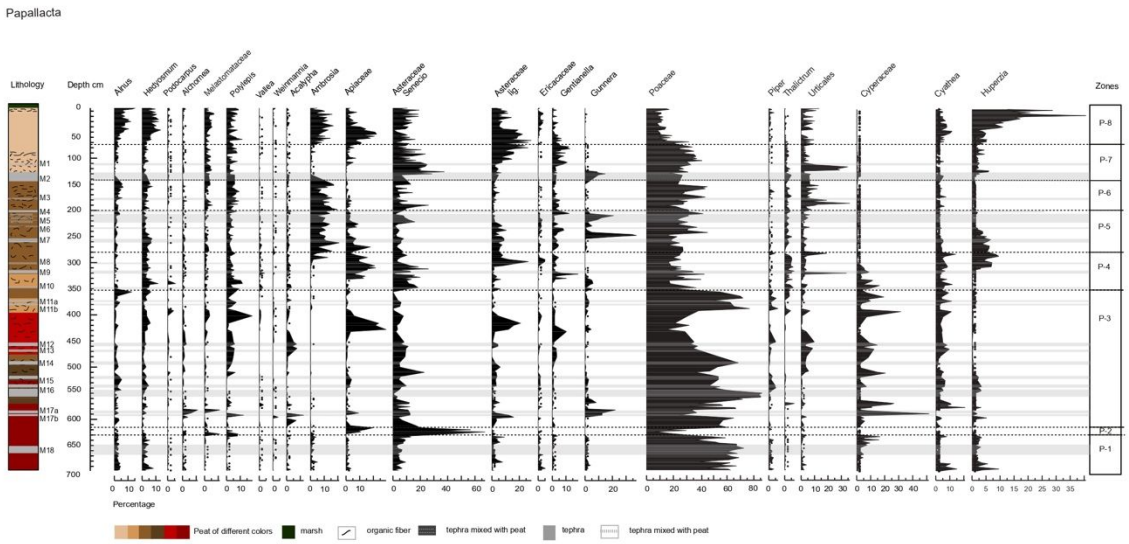

Figure 3: Percentages of 23 selected pollen and non-pollen taxa sampled in core PA1-08 plotted along a depth scale. Grey shaded areas indicate tephras; dashed horizontal lines: statistically significant pollen assemblage zone boundaries.

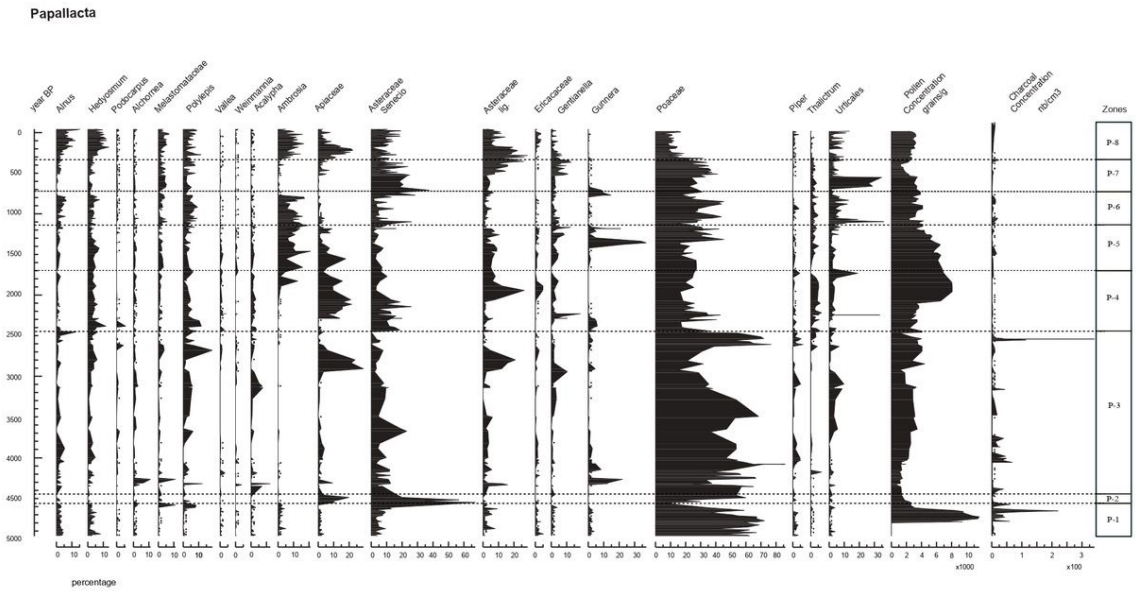

Figure 4: Percentages of 23 selected pollen and non-pollen taxa sampled from core PA1-08 plotted along an age scale. Dashed horizontal lines: statistically significant pollen assemblage zone boundaries

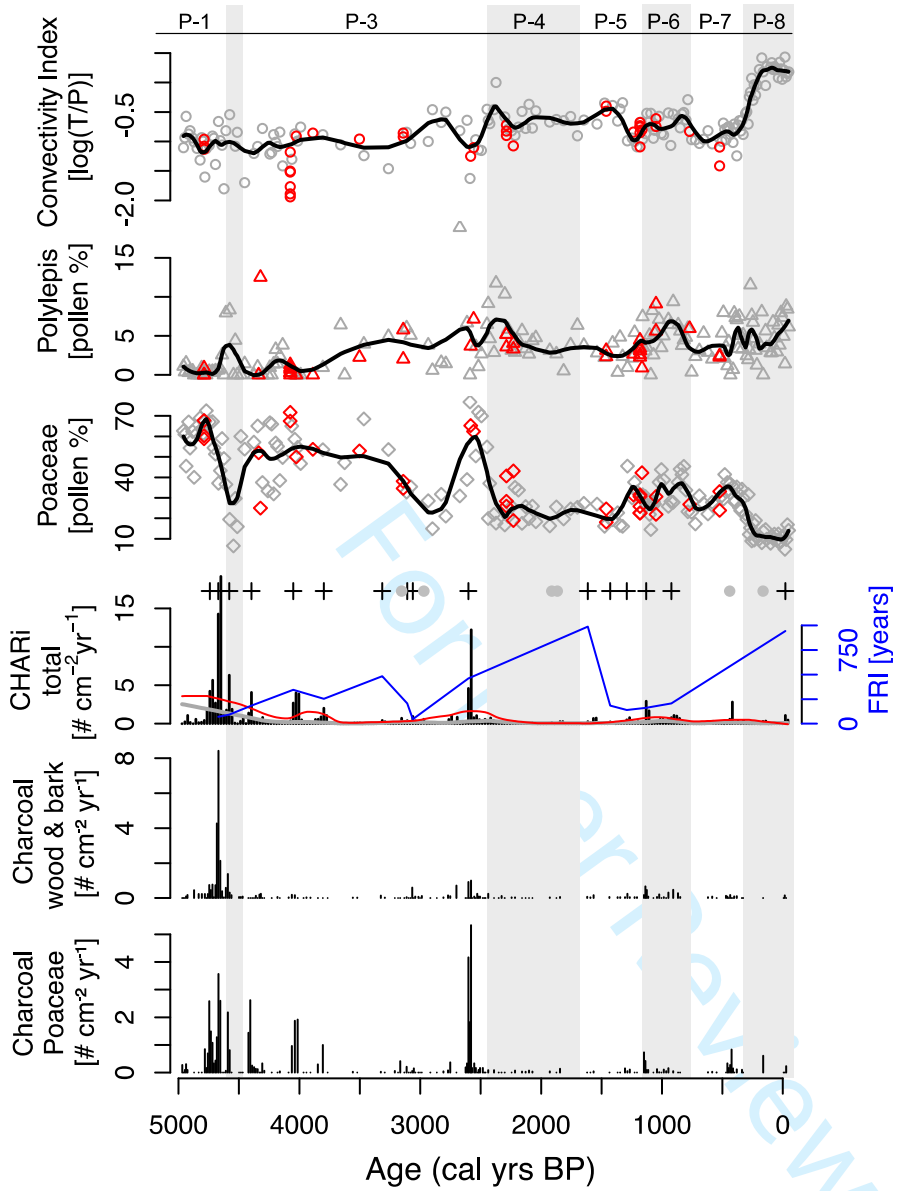

Figure 5: Results of core PA1-08. Comparison between vegetation dynamics and fire history in Papallacta bog. From top to bottom: the convective wind activity (convectivity index) inferred from the log-transformed Transported pollen:Poaceae pollen ratio (log(T/P)), *Polylepis* and Poaceae pollen percentages, and fire history based on the abundance of all particles of charcoal, wood and bark charcoal, and Poaceae charcoal. Red empty symbols: samples from tephra layers; black thick lines: loess smoothed records; histograms: charcoal accumulation rate; thick grey line: burned biomass; thin red line: threshold; crosses: fire events; gray circles: insignifanct charcoal peaks; blue line: fire return interval (FRI).

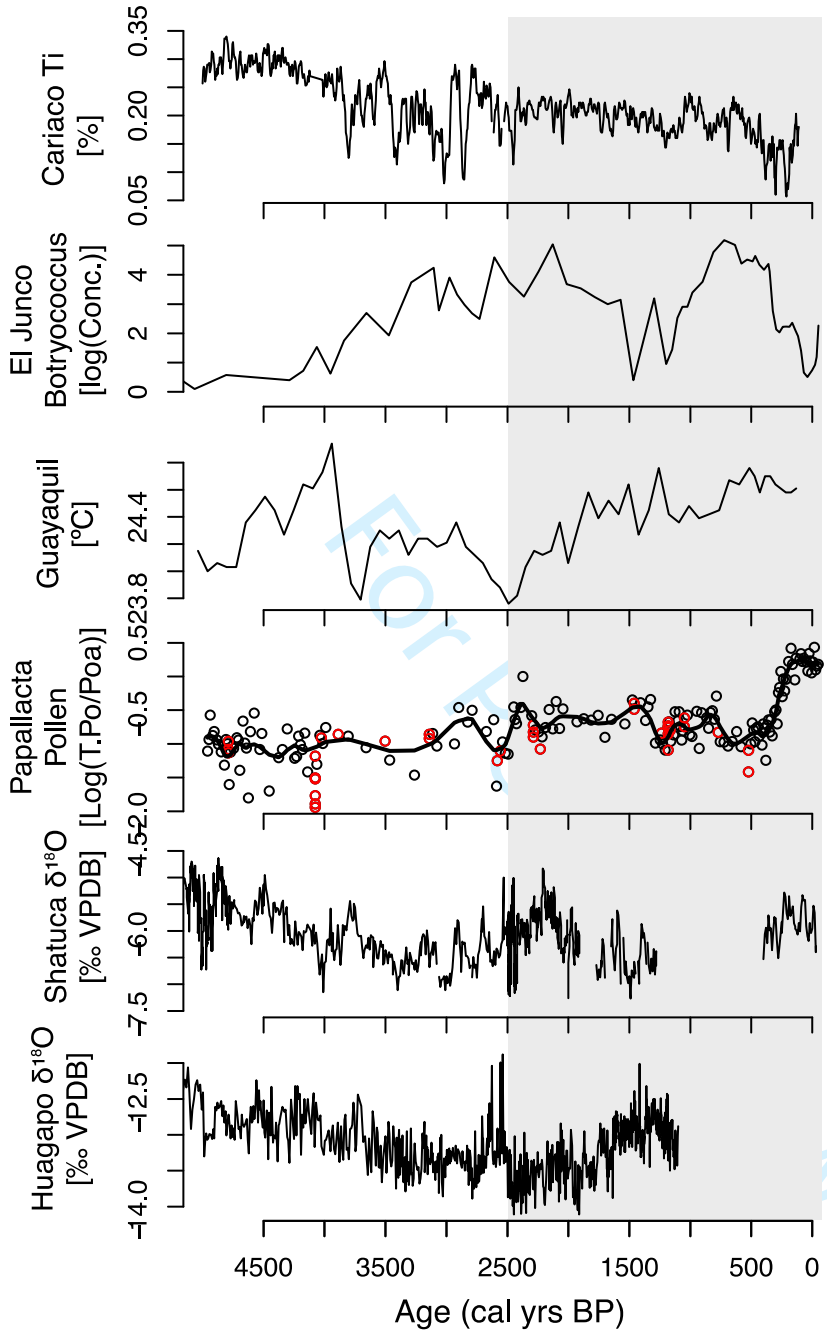

Figure 6: Records documenting past changes in precipitation in western tropical South America for the past 5,000 years. From north to south (A) the changes in Ti% associated with shifts in ITCZ at Cariaco (10°N) (Haug et al., 2001) (B)) changes in *Botrycoccus* frequencies at El Junco (Galapagos), a record of El Niño frequency (Zhang et al., 2014) (C) SST in the Bay of Guayaquil (Ecuador; Mollier-Vogel et al., 2013) (D) the Papallacta T/P index of upslope convective activity calculated from the PA1-08 pollen record; (E) changes in $\partial^{18}O$ at Shatuca (Peru): a record of SASM intensity (Bustamante et al., 2016); F) changes in ∂18O at Huagapo (Peru): a record of SASM intensity (Kanner et al., 2013).

Supplementary Table

Table S1 Radiocarbon ages of the eruptions dated *in situ* taken from volcanologic studies, including the location of the dated material inside (I), under (U) or above (O) the tephra, the link with the tephra layers observed at Papallacta and the associated references.

Sample number	Lab number	Material	Position	Age 14C	Reference
Tephra M1: 1560-1660 AD					
PICH-98C	GrN25522	charcoal	I	240 ± 20	Robin et al .,2008
PICH-98B1	GrN25521	charcoal	I	290 ± 20	
PICH-90A	GrN25517	charcoal	I	320 ± 20	
PICH-33B	GrA32951	charcoal	I	330 ± 30	
PICH-128B	GrA32953	charcoal	I	330 ± 30	
PICH-30G	GrN25508	charcoal	I	335 ± 20	
Tephra M2: Quilotoa					
	Beta analytic	charcoal	I	840 ± 50	Mothes and Hall, 2008
	USGS-M	charcoal	I	900 ± 150	
	USGS-M	charcoal	I	1150 ± 300	
	Teledyne isotopic	paleosoil	U	820 ± 80	
	Beta analytic	charcoal	I	770 ± 40	
	Beta analytic	charcoal	I	780 ± 40	
Tephra M3: 10th century eruption of the Guagua Pichincha					
PICH-36C	GrN30187	paleosoil	U	930 ± 60	Robin et al., 2008
PICH-127C	GrN30189	charcoal	I	1020 ± 25	
PICH-85	GrN25513	paleosoil	U	1100 ± 40	
PICH-87	GrN25515	charcoal	I	1100 ± 90	
PICH-38E	GrN24776	charcoal	I	1120 ± 30	
PICH-127B	GrN25809	charcoal	I	1180 ± 30	
PICH-127A	GrN26206	charcoal	I	1260 ± 70	
Tephra M4 (?): Cotopaxi "X" eruption					
		paleosoil	U	1180 ± 80	Hall and Mothes, 2008
		paleosoil	U	1210 ± 80	
Tephra M9-10: N6 eruption of the Atacazo-Ninahuilca					
SA-22E4	GrN28724	charcoal	I	2320 ± 30	Hidalgo et al., 2008
SA-22A	GrN28723	paleosoil	U	2300 ± 30	

SA-45B	GrN28730	charcoal	I	2260 ± 30	
SA-38C1	GrN28728	paleosoil	U	2250 ± 30	
SA-52B	GrN28731	charcoal	I	2230 ± 40	
SA-42D	GrN28729	charcoal	I	2220 ± 40	
Tephra M12 (?): Cuicocha eruption					
Tephra M13 (?): Tungurahua 3000 BP eruption					
		wood	I	2995 ± 90	Hall et al., 1999; Le Pennec et al 2013
	GrN27847	charcoal	I	2640 ± 45	
	GrA34159	charcoal	I	2845 ± 40	
	GrA23911	charcoal	I	2915 ± 40	
	GrA30884	charcoal	I	2960 ± 30	
	GrA33878	charcoal	I	3045 ± 45	
	GrA24128	charcoal	U	3195 ± 45	
Tephra M14-15 (?): Guagua Pichincha					
PICH-29B	GrN25507	charcoal	I	3540 ± 30	Robin et al., 2008
PICH-72	GrN25512	paleosoil	U	3700 ± 30	
Tephra M16: Cotopaxi rhyolites (F or Colorado canyon)					
		paleosoil	O	4420 ± 80	Hall and Mothes, 2008
		paleosoil	O	4670 ± 70	
		charcoal	I	4460 ± 140	
		paleosoil	O	4170 ± 110	
		paleosoil	O	3950 ± 70	
Tephra M18 (?): N5 eruption of the Atacazo-Ninahuilca					
SA-24C	GrN28725	charcoal	I	4360 ± 50	Hidalgo et al., 2008
SA-24I	GrN28726	charcoal	I	4440 ± 50	
SA-38A	GrN28727	paleosoil	U	4600 ± 40	
Tephra M18 (?): Chachimbiro eruption					
CHA-BB-016	SacA19708	peat overlying tephra dep	O	4615 ± 40	Bernard et al., 2014
CHA-BB-009	GrN32372	charcoal	I	4790 ± 65	
CHA-BB-021	GrN32373	charcoal	I	4766 ± 50	
CHA-BB-022	SacA19694	charcoal	I	4760 ± 40	

909
910

Table S2 Age of the tephra layers calculated from the age model based on the identification of the origin of the ash deposit reported in Table S1. Only three tephras showed no or little identification uncertainty and were included in the final age model (Fig. 2).

Papallaca PA1-08					Ages of the tephras based on documentary evidence and 14C dates			
Tephra ID	**TopDepth**	**BotDepth**	**Depth**	**Thickness**	**Cal BP**	**^{14}C BP**	**error**	**Uncertainty 0 no; 3 max**
M1	110	115	112.5	5	430		20	1
M2ab	130	148	139	18	793		24	0
M3	178	181	181	3	1096		15	1
M4	202	206	204	4		1210	200	2
M4	202	206	204	4		1230	30	2
M5	208	226	217	18		#N/A	#N/A	3
M6	232	236	234	4		#N/A	#N/A	3
M7	257	264	260.5	7		#N/A	#N/A	3
M8	318	322	320	4		#N/A	#N/A	3
M9	326	332	329	6		2320	30	3
M9	326	332	329	6		2300	30	3
M9	326	332	329	6		2260	30	3
M9	326	332	329	6		2250	30	3
M9	326	332	329	6		2230	40	3
M9	326	332	329	6		2220	40	3
M10	350	354	352	4		2320	30	3
M10	350	354	352	4		2300	30	3
M10	350	354	352	4		2260	30	3
M10	350	354	352	4		2250	30	3
M10	350	354	352	4		2230	40	3
M10	350	354	352	4		2220	40	3
M11a	374	377	375.5	3		2450	30	3
M11b	381	386	383.5	5		2520	30	3
M12	458	464	461	6		In progress		
M13	470	473	471.5	3		2995	90	3
M13	470	473	471.5	3		2640	45	3
M13	470	473	471.5	3		2845	40	3
M13	470	473	471.5	3		2915	40	3
M13	470	473	471.5	3		2960	30	3
M13	470	473	471.5	3		3045	45	3
M13	470	473	471.5	3		3195	45	3
M14	493	500	496.5	7		3540	30	3
M14	493	500	496.5	7		3700	30	3
M15	521	528	524.5	7		3540	30	3
M15	521	528	524.5	7		3700	30	3
M16a	538	542	540	4		4420	80	3
M16b	546	562	554	16		4670	70	3

M16b	546	562	554	16		4460	140	3
M16b	546	562	554	16		4170	110	3
M16b	546	562	554	16		3950	70	3
M17a	589	592	590.5	3		#N/A	#N/A	
M17b	594	596	595	2		#N/A	#N/A	
M18	658	668	663	10		4615	40	
M18	658	668	663	10		4790	65	
M18	658	668	663	10		4766	50	
M18	658	668	663	10		4760	40	
M18	658	668	663	10		4360	50	
M18	658	668	663	10		4440	50	
M18	658	668	663	10		4600	40	

Supplementary references

Bernard B, Hidalgo S, Robin C *et al.* (2014) The 3640–3510 BCrhyodacite eruption of Chachimbiro compound volcano, Ecuador: a violent directed blast produced by a satellite dome. *Bull Volcanol* 76: 849.

Hall ML, Mothes PA (2008) Quilotoa volcano—Ecuador: an overview of young dacitic volcanism in a lake-filled caldera. J Volcanol Geotherm Res 176:44–55. doi:10.1016/j.jvolgeores.2008.01.025

Hall, M., Mothes, P. The rhyolitic–andesitic eruptive history of Cotopaxi volcano, Ecuador. *Bull Volcanol* **70,** 675–702 (2008). https://doi.org/10.1007/s00445-007-0161-2

Hidalgo S, Monzier M, Almeida E, Chazot G, Eissen J-P, van der Plicht J, Hall ML (2008) Late Pleistocene and Holocene activity of the Atacazo–Ninahuilca volcanic complex (Ecuador). J Volcanol Geotherm Res 176:16–26. doi:10.1016/j.jvolgeores.2008.05.017

Robin C, Samaniego P, Le Pennec J-L, Mothes P, van der Plicht J (2008) Late Holocene phases of dome growth and Plinian activity at Guagua Pichincha volcano (Ecuador). J Volcanol Geotherm Res 176:7–15. doi:10.1016/j.jvolgeores.2007.10.008

Table 1. Description of the vegetation cover around Papallacta bog (from Ledru et al., 2013).

Site	Family	Species	Family	Species
Paramo 3,600- 4,000 m asl	Poaceae	*Calamagrostis sp.*	Asteraceae	*Diplostephium sp.*
		Festuca sp.		
	Rosaceae	*Polylepis sp.*		*Pentacalia sp.*
	Hypericaceae	*Hypericum sp.*		
Papallacta bog	Asteraceae	*Loricaria toyoides*	Gunneraceae	*Gunnera magellanica*
		Dorobaea pinpinelifolia	Ranunculaceae	*Ranunculus sp.*
3,815 m asl		*Monticalia vaccinioides*	Clusiaceae	*Hypericum laricifolium*
		Hippochoeris sp.		*Hypericum sp.*
		Xenophyllum sp.	Geraniaceae	*Geranium sp.*
		Werneria sp.	Polygonaceae	*Muehlenbeckia volcanica*
	Valerianaceae	*Valeriana microphylla*	Apiaceae	*Hydrocotyle sp.*
	Lycopodiaceae	*Huperzia sp.*		*Azorella sp.*
	Gentianaceae	*Gentiana sedifolia*	Plantaginaceae	*Plantago rigida*
		Halemia weddeliana	Cyperaceae	*Carex lechmanii*
		Gentianella sp.		
	Poaceae	*Cortaderia sericanta*		
		Bromus sp.		
		Cortaderia nitida		
Cushion paramo	Apiaceae	*Azorella sp.*	Plantaginaceae	*Plantago sp.*
Paramo >4,000 m asl	Malvaceae	*Nototriche sp.*	Brassicaceae	*Draba sp.*
	Apiaceae	*Azorella sp.*	Plantaginaceae	*Plantago sp.*
	Asteraceae	*Chuquiraga sp.*		
		Loricaria sp.		
		Werneria sp.		

Table 2. Radiocarbon dates of core PA1-08. Radiocarbon ages were measured on total organic matter. * = calendar age; ** = rejected 14C dates

Lab number	Depth cm	Age ^{14}C yr BP	Lab number	Depth cm	Age ^{14}C yr BP
surface	0-2	-60 ±10*			
SacA-11045	22-24	0 ±30	SacA-11050	494-496	3305±30
SacA-18852	50-52	175±30	SacA-18857	516-518	3180±40
Beta-243042	80-82	270±40	SacA-14728	524-526	3790±35
SacA-14722	114-116	530±30	SacA-11051	548-550	3690±30
SacA-14723	160-162	1005±30	SacA-18858	554-556	3790±30
SacA-11046	186-188	1000±30	SacA-14677	568-570	3950±40
SacA-11047	208-210	1105±30	SacA-11052	594-596	3570±30**
SacA-14724	254-256	1540±35	Beta-243043	602-604	3440±40**
SacA-18853	284-286	1860±30	SacA-14678	636-638	4475 ±40
SacA-18855	322-324	2225±40	SacA-18859	680-682	4330±30
SacA-11048	338-340	2470±30	SacA-14679	712-714	4600 ±50
SacA-18854	350-352	2440±30	SacA-18860	742-744	4560±40
SacA-14725	386-388	2885±35	SacA-11053	766-768	4380±30
SacA-14726	404-406	2520±35	SacA-18861	788-790	4460±35
SacA-11049	438-440	2950±30	SacA-14729	806-808	4430±40
SacA-18856	450-452	2885±30	SacA-14680	832-834	4290±40
SacA-14727	476-478	2935±35	SacA-11054	862-863	3620±30**

Tephra layer number	Depth cm	Cordillera	Volcano	Calibrated date of the eruption	Description of the ash layer	References
M1	110-115	WC	Guagua Pichincha	1600 AD	Fine, yellowish ash	Robin et al., 2008
M2a & b	130-148	WC	Quilotoa	1150 AD	2a white & 2b coarse grey ash with small pumice lapilli	Mothes and Hall 2008
M3	181	WC	Guagua Pichincha	975 AD	Coarse, crystal-rich ash with peat	Robin et al., 2008
M4	202-206	EC	Cotopaxi?	1165 yr BP	Yelllowish ash	Hall and Mothes 2008
M5	208-226	EC	Antisana	1180 yr BP	Peat with coarse ash and disseminated lapilli	
M6	232-236	-	-	1235 yr BP	Fine, yellowish ash with peat	
M7	257-264	EC	Cotopaxi?	1460 yr BP	Coarse, crystal-rich ash with peat	
M8	318-322	-	-	2230 yr BP	Fine-medium, grey-yellow, crystal-rich ash with peat	
M9	326-332	WC	Atac	2290 yr BP	Fine, white ash	Hidalgo et al., 2008
M10	350-354	-	-	2445 yr BP	Medium ash with peat	
M11a	374-377	-	-	2560 yr BP	Fine, grey-yellowish ash	
M11b	381-386	WC	-	2585 yr BP	Fine, grey-yellowish ash with disseminated lapilli	
M12	458-464	-	-	3140 yr BP	Fine-medium, white ash, well-stratified oxidation level	Hildebrandt 1989
M13	470-473	EC	Tungurahua	3195 yr BP	Medium ash with peat	Hall et al., 1999; Le Pennec et al., 2013
M14	493-500	-	-	3500 yr BP	Fine, clay-rich, dar ash with peat	
M15	521-528	WC	Pichincha	3890 yr BP	Medium, grey-white ash with disseminated crystals	Robin et al., 2008
M16	538-542 546-562	EC	Cotopaxi	4075 y BP	Fine-medium, pseudo-stratified ash with disseminated lapilli	Hall and Mothes 2008
M17a	589-592	WC	-	4320 yr BP	Fine, white ash	
M17b	594-596	WC	-	4335 yr BP	Medium, grey-yellowish ash	
M18	658-668	EC	Atacazo-Ninahuilca	4790 yr BP	Fine, white ash	Hidalgo et al., 2008

Supplementary table Radiocarbon ages of the eruptions dated in situ by the volcanologists with the location of the dated material I inside U under the tephra O above the tephra, the link with the tephra layers observed at Papallacta and the associated references.

Sample number	Lab number	Material	Position	Age 14C	Reference
Tephra M1: 1560-1660 AD					
PICH-98C	GrN25522	charcoal	I	240 ± 20	Robin et al .,2008
PICH-98B1	GrN25521	charcoal	I	290 ± 20	
PICH-90A	GrN25517	charcoal	I	320 ± 20	
PICH-33B	GrA32951	charcoal	I	330 ± 30	
PICH-128B	GrA32953	charcoal	I	330 ± 30	
PICH-30G	GrN25508	charcoal	I	335 ± 20	
Tephra M2: Quilotoa					
	Beta analytic	charcoal	I	840 ± 50	Mothes and Hall, 2008
	USGS-M	charcoal	I	900 ± 150	
	USGS-M	charcoal	I	1150 ± 300	
	Teledyne isotopic	paleosoil	U	820 ± 80	
	Beta analytic	charcoal	I	770 ± 40	
	Beta analytic	charcoal	I	780 ± 40	
Tephra M3: 10th century eruption of the Guagua Pichincha					
PICH-36C	GrN30187	paleosoil	U	930 ± 60	Robin et al., 2008
PICH-127C	GrN30189	charcoal	I	1020 ± 25	
PICH-85	GrN25513	paleosoil	U	1100 ± 40	

PICH-87	GrN25515	charcoal	I	1100 ± 90	
PICH-38E	GrN24776	charcoal	I	1120 ± 30	
PICH-127B	GrN25809	charcoal	I	1180 ± 30	
PICH-127A	GrN26206	charcoal	I	1260 ± 70	
Tephra M4 (?): Cotopaxi "X" eruption					
		paleosoil	U	1180 ± 80	Hall and Mothes, 2008
		paleosoil	U	1210 ± 80	
Tephra M9-10: N6 eruption of the Atacazo-Ninahuilca					
SA-22E4	GrN28724	charcoal	I	2320 ± 30	Hidalgo et al., 2008
SA-22A	GrN28723	paleosoil	U	2300 ± 30	
SA-45B	GrN28730	charcoal	I	2260 ± 30	
SA-38C1	GrN28728	paleosoil	U	2250 ± 30	
SA-52B	GrN28731	charcoal	I	2230 ± 40	
SA-42D	GrN28729	charcoal	I	2220 ± 40	
Tephra M12 (?): Cuicocha eruption					
Tephra M13 (?): Tungurahua 3000 BP eruption					
		wood	I	2995 ± 90	Hall et al., 1999; Le Pennec et al., 2013
	GrN27847	charcoal	I	2640 ± 45	
	GrA34159	charcoal	I	2845 ± 40	
	GrA23911	charcoal	I	2915 ± 40	
	GrA30884	charcoal	I	2960 ± 30	
	GrA33878	charcoal	I	3045 ± 45	
	GrA24128	charcoal	U	3195 ± 45	
Tephra M14-15 (?): Guagua Pichincha					

PICH-29B	GrN25507	charcoal	I	3540 ± 30	Robin et al., 2008
PICH-72	GrN25512	paleosoil	U	3700 ± 30	
Tephra M16: Cotopaxi rhyolites (F or Colorado canyon)					
		paleosoil	O	4420 ± 80	Hall and Mothes, 2008
		paleosoil	O	4670 ± 70	
		charcoal	I	4460 ± 140	
		paleosoil	O	4170 ± 110	
		paleosoil	O	3950 ± 70	
Tephra M18 (?): N5 eruption of the Atacazo-Ninahuilca					
SA-24C	GrN28725	charcoal	I	4360 ± 50	Hidalgo et al., 2008
SA-24I	GrN28726	charcoal	I	4440 ± 50	
SA-38A	GrN28727	paleosoil	U	4600 ± 40	
Tephra M18 (?): Chachimbiro eruption					
CHA-BB-016	SacA19708	peat overlying tephra dep	O	4615 ± 40	Bernard et al., 2014
CHA-BB-009	GrN32372	charcoal	I	4790 ± 65	
CHA-BB-021	GrN32373	charcoal	I	4766 ± 50	
CHA-BB-022	SacA19694	charcoal	I	4760 ± 40	

References

Bernard B, Hidalgo S, Robin C *et al.* (2014) The 3640–3510 BCrhyodacite eruption of Chachimbiro compound volcano, Ecuador: a violent directed blast produced by a satellite dome. *Bull Volcanol* 76: 849.

Hall ML, Mothes PA (2008) Quilotoa volcano—Ecuador: an overview of young dacitic volcanism in a lake-filled caldera. J Volcanol Geotherm Res 176:44–55. doi:10.1016/j.jvolgeores.2008.01.025

Hall, M., Mothes, P. The rhyolitic–andesitic eruptive history of Cotopaxi volcano, Ecuador. *Bull Volcanol* **70,** 675–702 (2008). https://doi.org/10.1007/s00445-007-0161-2

Hidalgo S, Monzier M, Almeida E, Chazot G, Eissen J-P, van der Plicht J, Hall ML (2008) Late Pleistocene and Holocene activity of the Atacazo–Ninahuilca volcanic complex (Ecuador). J Volcanol Geotherm Res 176:16–26. doi:10.1016/j.jvolgeores.2008.05.017

Robin C, Samaniego P, Le Pennec J-L, Mothes P, van der Plicht J (2008) Late Holocene phases of dome growth and Plinian activity at Guagua Pichincha volcano (Ecuador). J Volcanol Geotherm Res 176:7–15. doi:10.1016/j.jvolgeores.2007.10.008

von Hillebrandt C (1989) Estudio geovolcanológico del Complejo Volcánico Cuicocha-Cotacachi y sus aplicaciones. Provincia de Imbabura, Tesis de Ingeniería, Escuela Politécnica Nacional, Quito-Ecuador

Table S2 Age of the tephra layers calculated from the age model based on the identification of the origin of the ash deposit reported in Table S1. Only three tephras showed no or little identification uncertainty and were included in the final age model (Fig. 2).

Papallaca PA1-08					Ages of the tephras based on documentary evidence and 14C dates			
Tephra ID	**TopDepth**	**BotDepth**	**Depth**	**Thickness**	**Cal BP**	**^{14}C BP**	**error**	**Uncertainty 0 no; 3 max**
M1	110	115	112.5	5	430		20	1
M2ab	130	148	139	18	793		24	0
M3	178	181	181	3	1096		15	1
M4	202	206	204	4		1210	200	2
M4	202	206	204	4		1230	30	2
M5	208	226	217	18		#N/A	#N/A	3
M6	232	236	234	4		#N/A	#N/A	3
M7	257	264	260.5	7		#N/A	#N/A	3
M8	318	322	320	4		#N/A	#N/A	3
M9	326	332	329	6		2320	30	3
M9	326	332	329	6		2300	30	3
M9	326	332	329	6		2260	30	3
M9	326	332	329	6		2250	30	3
M9	326	332	329	6		2230	40	3
M9	326	332	329	6		2220	40	3
M10	350	354	352	4		2320	30	3
M10	350	354	352	4		2300	30	3
M10	350	354	352	4		2260	30	3
M10	350	354	352	4		2250	30	3
M10	350	354	352	4		2230	40	3
M10	350	354	352	4		2220	40	3
M11a	374	377	375.5	3		2450	30	3
M11b	381	386	383.5	5		2520	30	3
M12	458	464	461	6		2980	30	3
M13	470	473	471.5	3		2995	90	3
M13	470	473	471.5	3		2640	45	3
M13	470	473	471.5	3		2845	40	3
M13	470	473	471.5	3		2915	40	3
M13	470	473	471.5	3		2960	30	3
M13	470	473	471.5	3		3045	45	3
M13	470	473	471.5	3		3195	45	3
M14	493	500	496.5	7		3540	30	3
M14	493	500	496.5	7		3700	30	3
M15	521	528	524.5	7		3540	30	3
M15	521	528	524.5	7		3700	30	3
M16a	538	542	540	4		4420	80	3
M16b	546	562	554	16		4670	70	3

M16b	546	562	554	16		4460	140	3
M16b	546	562	554	16		4170	110	3
M16b	546	562	554	16		3950	70	3
M17a	589	592	590.5	3		#N/A	#N/A	
M17b	594	596	595	2		#N/A	#N/A	
M18	658	668	663	10		4615	40	
M18	658	668	663	10		4790	65	
M18	658	668	663	10		4766	50	
M18	658	668	663	10		4760	40	
M18	658	668	663	10		4360	50	
M18	658	668	663	10		4440	50	
M18	658	668	663	10		4600	40	